Modelling and Quantifying the Martingale Defect in Asset Price Bubbles

Elliot Jones

University of Bath

A thesis submitted in partial fulfilment for the degree of

Financial Mathematics with Data Science

Supervised by

Alex Cox

2025/2026

Contents

Abstract

Asset price bubbles represent persistent deviations from fundamental values that can precipitate systematic crises. Deeply rooted in history from instances such as the 1990s Dot-Com bubble and 2008 financial crisis, it appears that events like these are unavoidable and a constant reoccurrence. As such, the need for forward-looking detection is extremely sought after by regulators and financial institutions to manage this risk before it becomes collateral damage. The work within this thesis aims to build upon this need, presenting and implementing different techniques for bubble detection. Building upon martingale theory, we present three complementary estimation methods, including a tail average, mean shortfall, and Delta band estimator allowing for real market application. We analyse three pricing models to establish bubble-generating conditions. The Blacks-Scholes supports evidence of no bubbles present whereas the local and stochastic volatility models, CEV and SABR respectively, show evidence of a bubble present. Crucially, we demonstrate that the observed call option prices exhibit a strike independent plateau at far out-of-the-money (OTM) levels equal to the size of the bubble. This identity is then utilised on Nvidia options data which reveals a positive martingale defect across multiple maturities and Delta bands, suggesting potential bubble behaviour in live markets. Finally, we introduce a novel way to simulate a self-exciting pure-jump process whose exponential exhibits a strict local martingale, illustrating how real-world discontinuities and feedback dynamics amplify bubble risk. Together, these contributions deliver a practical, and easily implementable system for real-time bubble detection using only observed option prices.

Statement of Originality

DECLARATION This dissertation is submitted to the University of Bath in accordance with the requirements of the degree of MSc in Financial Mathematics With Data Science in the Department of mathematics. No portion of the work in this thesis has been submitted in support of an application for any other degree or qualification of this or any other university or institution of learning. Except where specifically acknowledged, it is the work of the author.

Signature of Author: Elliot Jones

Introduction

In modern financial theory, it is expected that asset prices should reflect all available information about them along with any accompanying risks. This notion, often cited as an asset's fundamental value, captures the fair price a rational investor would be willing to pay. Economic theory offers several complementary ways that define an assets fundamental value. Discounted cash flow (DCF) methods, treat value as the present value of expected cash flows under a risk-adjusted rate. Likewise, the dividend discount model defines fundamental value directly from the stream of expected dividends under a long run growth assumption. In A Random Walk Down Wall Street, Malkiel (2019) contrasts two valuation views. The firm-foundation view seeks an intrinsic value from fundamentals-balance-sheet strength, expected dividends, and growth prospects. Whereas, the castle-in-the-air (or greater-fool) view instead says that an asset is worth whatever another investor is willing to pay. Because fundamental value is somewhat subjective and can be computed in different ways, their estimates naturally diverge from market prices when investors hold heterogeneous beliefs. Market prices reflect the mix of these views, risk appetites, and constraints that converge where buy and sell orders balance. Bullish investors will be willing to bid higher while bearish investors demand a discount. Within normal no arbitrage bands, such dispersion is normal and expected. However, there are times when prices exhibit large, persistent departures from fundamentals that cannot be reconciled with any reasonable range of cash-flow forecasts, discount rate assumptions, or trading frictions. It is these sustained, economically meaningful excesses that we refer to as bubbles.

Explicitly, the formation of a bubble is commonly fuelled by excessive investor optimism and extreme speculative behaviour. Rapidly rising prices attract further demand due to economical phenomena such as herding and fear of missing out (FOMO), creating a self-reinforcing feedback loop pushing prices further away from fundamental ranges. After achieving unsustainable highs, bubbles are often followed by a sharp decline known as the bubble "burst". Kindleberger and Aliber (2005) characterises these bubbles as a sequence of five phases known as displacement, boom, euphoria, financial distress, and panic/crash. First, a displacement (e.g. a new technology or policy shift) alters profit expectations and attracts early investors. Rising prices then invite leverage and broader participation, fuelling a boom. Euphoria follows as valuation discipline weakens, momentum and herding dominate, and "this time is different" narratives take hold. Strains accumulate into

financial distress as funding tightens, insiders take profits, and failures surface. Finally, revulsion gives way to panic, lenders pull back, buyers vanish, liquidity evaporates, and prices overshoot downward ending in a crash. Although this pattern is re-occurring it is only once the bubble has taken place that these stages can be identified with some stages being blurred, skipped, or compressed.

When bubbles collapse, there is a real risk that they can precipitate broader financial crises not only affecting investors but also the wider economy. Historical instances such as the U.S. housing market bubble in 2007-2008 highlight this, where risky mortgage lending and securitization led to a massive global credit crunch, multiple bank failures and a worldwide recession. This negligence left millions of Americans homeless and many more unemployed demonstrating the indirect impact that asset bubbles can have on the broader economy Singh (2024). Similarly, the late-1990s Dot-Com episode saw equity valuations for internet firms surge on optimistic growth narratives and momentum-driven flows before collapsing in 2000, causing large wealth losses and a sectoral shake-out Shiller (2000); Ofek and Richardson (2003).

Episodes like these matter for two reasons. First, they show how credit, funding structures, and feedback trading can transform pricing errors into systemic risk, with losses transmitted beyond investors to households and firms. Secondly, they expose a persistent measurement problem, post classification is straightforward, but real time identification poses a challenge. The need is therefore for forward-looking, market-based diagnostics that can operate with realistically available data and are compatible with no-arbitrage pricing.

Highlighted by their significance in affecting market dynamics, financial bubbles have influenced both the evolution of economic theory and the development of financial regulation. Their recurring presence in financial history has spurred increased efforts among policymakers, economists, and financial institutions to understand the behavioural and structural causes behind such phenomena. As a result, frameworks such as macro-prudential regulation, stress testing, and early warning indicators have been developed to mitigate systemic risk and enhance financial stability. This study builds upon this to identify a sustained non-fundamental price component in real time using market data. In particular, we develop option-implied, no arbitrage diagnostics designed to work with realistically available quotes to potentially flag and measure such components before they have occurred.

Chapter 1

Theoretical Background of Asset Bubble Detection

Modelling financial bubbles poses a fundamental challenge. We want to describe episodes in which market prices persistently outstrip fundamental value without permitting easy arbitrage. This creates a tension, as no-arbitrage is the organising principle of modern asset pricing, yet bubble phases exhibit seemingly explosive run-ups and sharp corrections that make it look like a free lunch is possible. Our aim is to reconcile these features by adopting a framework that allows bubble-like behaviour while still excluding easy arbitrage strategies. We work under a minimal no arbitrage baseline and take a risk neutral viewpoint in which the discounted price may evolve in a way that generates a measurable mispricing relative to the fundamental value, emphasising the idea that one can permit paths that look explosive without creating trading strategies that give a free lunch. Under basic no arbitrage conditions of option quotes (monotonicity, convexity, and parity), the call surface reveals a strike-independent plateau of which identifies the mispricing represented between the fundamental and actual value of the asset, while puts continue to reflect fundamentals. These identities underpin the estimators and empirical tests used later in the thesis.

1.1 How to define a bubble

Having established the economic nature and significance of asset bubbles, we wish to expand on this and develop the mathematical framework necessary for their detection. The challenge is to translate the intuitive notion of when market prices exceed fundamental value into a rigorous and testable mathematical criterion while ensuring no-arbitrage conditions hold. This creates a conflict, as we wish to have asset prices that run persistently above any reasonable estimate of intrinsic value while ensuring that no free lunch exists. An arbitrage strategy can be defined as a trading strategy that requires no initial investment, carries no risk of loss, and delivers a strictly positive probability of a gain. If

such opportunities were to exist, rational investors would exploit these continuously forcing prices to adjust until this arbitrage opportunity has been priced away. This leads to the classical no arbitrage condition which states that, there exists a probability measure $\mathbb{Q}$, equivalent to the real world measure $\mathbb{P}$, under which every discounted asset price $S_t = e^{-rt}S_t$ is a martingale (Delbaen and Schachermayer, 1994). We define a martingale formally as such,

Definition 1.1.1. *(Martingale) Given a filtered probability space* $(\Omega, \mathcal{F}, \{\mathcal{F}_t\}_{t\geq 0}, \mathbb{P})$ *and a continuous time stochastic process*

$$M : \Omega \times [0, +T) \to \mathbb{R}^d, \tag{1.1.1}$$

we say that M *is an* $\{\mathcal{F}_t\}_{t\geq 0}$ *martingale if:*
i) For all $t \geq 0$

$$\mathbb{E}_{\mathbb{Q}}[|M_t|] < +\infty, \tag{1.1.2}$$

ii) for all $0 \leq s \leq t < +\infty$

$$\mathbb{E}_{\mathbb{Q}}[M_t|\mathcal{F}_s] = M_s\,. \tag{1.1.3}$$

Under this simple no-arbitrage framework, every asset price is equal to its expected discounted payoff under the unique martingale measure $\mathbb{Q}$. In particular, under zero interest and zero dividends $(r = 0, d = 0)$,

$$S_t = \mathbb{E}_{\mathbb{Q}}[S_T|\mathcal{F}_t] \tag{1.1.4}$$

However, this classical condition is too restrictive to allow for bubbles. It assumes perfect market completeness and unconstrained trading, which real markets often violate (Delbaen and Schachermayer, 1994; Jarrow, Protter and Shimbo, 2010). This means that persistent overvaluation observed from bubble episodes would be arbitraged away if every trader could borrow and short sell. To model bubbles, we must refine this no arbitrage condition beyond the simple martingale requirement to allow for more realistic market conditions. To do this we follow the market framework as in Jarrow, Protter and Shimbo (2006).

We model an economy consisting of a risky asset, whose ex-dividend price is denoted by S_t, a càdlàg semimartingale $(D_t)_{0\leq t<\tau}$ that represents the cumulative dividends up to time t, the terminal payoff X_τ at time τ where τ is the maturity of the risky asset, and a money market account with zero interest so that it has constant value. The market price of the risky asset $S = (S_t)_{t\geq 0}$ is represented by a nonnegative càdlàg semimartingale. We assume that $X_\tau, D_t \geq 0$, for each $t \in (0, \tau)$ and that all processes are defined on a filtered

probability space $(\Omega, \mathcal{F}, \mathcal{F}_t, \mathbb{P})$ satisfying the same conditions as in Jarrow, Protter and Shimbo (2006). The wealth process $W = (W_t)_{t\geq 0}$ of holding one share of the risky asset up to time t is then

$$W_t = S_t + \int_0^{t\wedge\tau} dD_u + X_\tau \mathbf{1}_{\{\tau\leq t\}}. \tag{1.1.5}$$

Having specified the economy, we define the self-financing trading strategy as a predictable pair of processes $(\pi, \eta) = (\pi_t, \eta_t)_{t\geq 0}$, where π_t denotes the number of shares of the risky asset held at time t, and η_t is the cash balance in a zero-interest money market account. Choosing the value of the initial investment to be null ($V_0 = 0$) and assuming that π is predictable and W-integrable, the wealth of such trading strategy evolves according to

$$V_t^{\pi,\eta} = \pi_t S_t + \eta_t = \int_0^t \pi_u dW_u. \tag{1.1.6}$$

$$\text{Where} \quad \eta = \int_0^{t\wedge\tau} \pi_u dD_u + \pi_\tau X_\tau \mathbf{1}_{\{\tau\leq t\}} - \int_0^t S_{u-} d\pi_u - [\pi^c, S^c]_t, \quad \eta_0 = -\pi_0 S_0, \tag{1.1.7}$$

as derived in Jarrow, Protter and Shimbo (2006). Here, $[\pi^c, S^c]_t$ represents the quadratic covariation between the continuous local-martingale part of π and S left over after we applied Itó's formula to (1.1.6). Additionally, we restrict our attention to admissible, self-financing trading strategies to rule out unbounded doubling strategies.

Definition 1.1.2. *(Admissibility) Let $V^{\pi,\eta}$ be the wealth process given by (1.1.6) we say that the trading strategy π is admissible if it is self-financing and $V_t^{\pi,\eta} \geq -a$ a.s. for all $t \geq 0$.*

Put simply, this notion of admissibility can be seen as a lower bound on the wealth process, forbidding the ability to borrow if one's debt becomes too large.

Let W denote the discounted vector price process and let π be a predictable W-integrable trading strategy. For zero initial capital, the self-financing gain process is $(\pi\cdot W)_t$, so the terminal gain is $W_\infty^\pi := (\pi\cdot W)_\infty$. We define

$$\mathcal{K} \;=\; \{\, W_\infty^\pi = (\pi\cdot W)_\infty \;:\; \pi \text{ is admissible} \,\}. \tag{1.1.8}$$

Thus $\mathcal{K}$ is the set of all terminal payoffs one can generate from zero cost using admissible strategies (Jarrow, Protter and Shimbo, 2006). Writing L_+^0 for the set of nonnegative random variables and L_∞ for bounded claims we define,

$$\mathcal{C} \;=\; (\mathcal{K} - L_+^0) \cap L_\infty. \tag{1.1.9}$$

Equivalently,

$$\mathcal{C} = \{\, X \in L_\infty \;:\; \exists Y \in \mathcal{K} \text{ with } X \leq Y \text{ a.s.} \,\}.$$

Therefore, $\mathcal{C}$ consists of all bounded payoffs that can be super-replicable at zero cost (i.e. you can trade to some $Y \in \mathcal{K}$ and, if necessary, discard a nonnegative remainder $U \geq 0$ so that $X = Y - U \leq Y$), and by construction, $\mathcal{C}$ is a convex cone (Jarrow, Protter and Shimbo, 2006). Having specified an admissible, self-financing strategy, we now impose the No Free Lunch with Vanishing Risk (NFLVR) condition to rule out any arbitrage opportunities.

Definition 1.1.3. *(No Free Lunch With Vanishing Risk) We say that a semimartingale S satisfies the NFLVR condition with respect to admissible integrands if,*

$$\bar{C} \cap L^\infty_+ = \{0\}. \tag{1.1.8}$$

Where $\bar{C}$ denotes the closure of C in the sup-norm topology of L^∞.

NFLVR is a fundamental concept in modern mathematical finance and serves as a cornerstone for the First Fundamental Theorem of Asset Pricing. In continuous time, NFLVR establishes the equivalence between the absence of arbitrage opportunities and the existence of an Equivalent Local Martingale Measure (ELMM) for asset prices.

Definition 1.1.4. *(Equivalent Local Martingale Measure (ELMM)). Let $(\Omega, \mathcal{F},)$ be a filtered complete probability space. An Equivalent Local Martingale Measure (ELMM) for a wealth process W is a probability measure $\mathbb{Q}$ equivalent to $\mathbb{P}$ on $\mathcal{F}_T$ such that W is a local $\mathcal{Q}$-martingale. We denote $\mathcal{M}_{loc}(W)$ the set of all $ELMMs$ for W.*

NFLVR provides the necessary theoretical foundation for the existence of asset price bubbles, which are otherwise excluded by simpler arbitrage-free conditions often applied in classical models. Informally, it rules out sequences of admissible, self-financing strategies whose downside risk vanishes while retaining a strictly positive payoff with nonzero probability. Thus, NFLVR excludes a broader range of non-standard strategies and trading practices than a simple "no arbitrage" condition.

Theorem 1.1.5. *(Fundamental Theorem of Asset Pricing) A market satisfies the No Free Lunch with Vanishing Risk (NFLVR) condition if and only if there exists an Equivalent Local Martingale Measure (ELMM).*

By Theorem 1.1.5, NFLVR holds if and only if there exists an ELMM $\mathbb{Q}$ under which the discounted price is a $\mathbb{Q}$-local martingale. Given that asset prices are non-negative (bounded below by zero), any non-negative local martingale is a super martingale and is therefore a true martingale or a strict local martingale. This implies that, under NFLVR, the price process of an asset can indeed be either a true martingale or a strict local martingale, allowing assets to possess bubbles.

Definition 1.1.6. *(Stopping time) Given a filtered probability space* $(\Omega, \mathcal{F}, \{\mathcal{F}_t\}_{t\geq 0}, \mathbb{P})$*, a random variable*

$$\tau : \Omega \mapsto [0, +\infty) \tag{1.1.9}$$

is called an $\{\mathcal{F}_t\}_{t\geq 0}$*-stopping time if*

$$\{\omega \in \Omega : \tau(\omega) \leq t\} \subset \mathcal{F}_t, \qquad \text{for all } t \in [0, +\infty). \tag{1.1.10}$$

Definition 1.1.7. *(Local Martingale) Given a filtered probability space* $(\Omega, \mathcal{F}, \{\mathcal{F}_t\}_{t\geq 0}, \mathbb{P})$*, a stochastic process*

$$M : \Omega \times [0, +\infty) \mapsto \mathbb{R}^d \tag{1.1.11}$$

is called a local martingale if there exists a sequence

$$\tau^n : \Omega \mapsto [0, +\infty) \qquad \text{for } n \geq 0 \tag{1.1.12}$$

of $\{\mathcal{F}_t\}_{t\geq 0}$ *- stopping times such that:*

i) $\mathbb{P}(\tau^n \leq \tau^{n+1}) = 1$,

ii) $\mathbb{P}(\lim_{n\mapsto\infty} \tau^n = +\infty) = 1$,

and the stopped process

$$t \mapsto M_t^{\tau^n} := M_{\tau^n \wedge t} \tag{1.1.13}$$

is an $\{\mathcal{F}_t\}_{t\geq 0}$*-martingale.*

In essence, M is a local martingale if it exhibits the martingale property until each τ_n but does not satisfy this globally. If, despite this localized behaviour, M still fails to satisfy the martingale property over the entire time horizon, we call it a strict local martingale. By Theorem 1.1.5, NFLVR holds if there exists an ELMM $\mathbb{Q}$ under which the discounted price is a $\mathbb{Q}$-local martingale. From this, we defined the fundamental price under this measure as,

Definition 1.1.8. *(Fundamental Price). The fundamental price* S_t^* *of an asset with market price* S_t *is defined by*

$$S_t^* = E_{\mathbb{Q}}\left[\int_t^\tau dD_u + X_\tau \mathbf{1}_{\{\tau<\infty\}} \middle| \mathcal{F}_t \right] \mathbf{1}_{\{t<\tau\}} \tag{1.1.14}$$

From now on we work in discounted units under a fixed $\mathbb{Q}$, and consider a single asset S with $D = 0$. Under this measure, the asset has a unique fundamental value given by $S_t^* = \mathbb{E}_{\mathbb{Q}}[S_T|\mathcal{F}_t]$ The goal now is to understand what "no easy arbitrage" (NFLVR) actually implies for the behaviour of S.

Proposition 1.1.9 (Nonnegative local martingale ⇒ supermartingale)**.** *Let $S \geq 0$ be a $\mathbb{Q}$–local martingale. Then for all $0 \leq t \leq T$,*

$$\mathbb{E}_{\mathbb{Q}}[S_T \mid \mathcal{F}_t] \leq S_t \quad a.s. \tag{1.1.15}$$

Proof. Let (τ_n) be a localization sequence so that S^{τ_n} is a $\mathbb{Q}$-martingale for each n. Since $S \geq 0$ and $\tau_n \uparrow \infty$, we have $S_{T\wedge\tau_n} \uparrow S_T$ a.s. Hence, by conditional Fatou's lemma as in Revuz and Yor (1999),

$$\mathbb{E}_{\mathbb{Q}}[S_T \mid \mathcal{F}_t] = \mathbb{E}_{\mathbb{Q}}[\lim_n S_{T\wedge\tau_n} \mid \mathcal{F}_t] \leq \liminf_n \mathbb{E}_{\mathbb{Q}}[S_{T\wedge\tau_n} \mid \mathcal{F}_t] = \liminf_n S_{t\wedge\tau_n} = S_t. \tag{1.1.16}$$

For fixed t, eventually $\tau_n > t$, so $t \wedge \tau_n = t$ and $\lim_n S_{t\wedge\tau_n} = S_t$ a.s. □

Either this inequality is an equality for all T (then S is a true martingale, i.e. $\mathbb{E}_{\mathbb{Q}}[S_T \mid \mathcal{F}_t] = S_t$), or it is strict for some T (then S is a strict local martingale, i.e. $\mathbb{E}_{\mathbb{Q}}[S_T \mid \mathcal{F}_t] < S_t$). This inequality suggests measuring overvaluation by the shortfall between the underlying assets true price and its ELMM expectation. We define this as the martingale defect, also known as the bubble gap Revuz and Yor (1999).

Definition 1.1.10. *(martingale defect / bubble gap)*

$$m(T) \;=\; S_0 - \mathbb{E}_{\mathbb{Q}}[S_T|\mathcal{F}_t] \;\geq\; 0. \tag{1.1.17}$$

Then $m(T) > 0$ for some T iff *S is a* strict *local martingale under $\mathbb{Q}$.*

Having formalised that the overvaluation in our no arbitrage framework is due to the presence of strict local martingales, we can now formally define a bubble,

Definition 1.1.11. *(Financial bubbles) The price process S has a bubble if S is a strict local martingale under the risk-neutral measure $\mathbb{Q}$.*

This method that we have introduced is commonly known as the local martingale approach in literature (Cox and Hobson, 2005; Jarrow, Protter and Shimbo, 2006). However, this is not the only approach for pricing bubbles. Another popular approach from Gilles (1989) introduces the notion of bubbles as charges. The framework in this method defines a financial bubble as a "charge" which represents an additional, non-fundamental component in the asset's price. Under the standard No Free Lunch theorem with vanishing risk (Jarrow, Protter and Shimbo (2006)) demonstrate that every asset price St admits a

unique decomposition into its fundamental value Ft and a non-negative speculative bubble component $C_t \geq 0$. This decomposition is expressed as

$$S_t = F_t + C_t. \tag{1.1.18}$$

Crucially, Jarrow, Protter and Shimbo (2006) prove that this "bubble as charge" definition is equivalent to the strict local martingale criterion. Therefore, while conceptually distinct in its initial formulation, the charges approach ultimately aligns with the martingale approach that forms the core of this research. We adopt the local martingale approach from Cox and Hobson (2005) for its tighter integration with arbitrage pricing theory and stochastic process modelling.

Jarrow, Protter and Shimbo (2006) classify bubbles into three distinct categories, labeled as type 1, type 2 and type 3 bubbles. Type 1 bubbles arise when the discounted price is a uniformly integrable local martingale and exist when an asset has an infinite life with a payoff $\{\tau = \infty\}$. Type 2 bubbles arise when the discounted price is a local martingale that is not uniformly integrable, which happens when the asset has a finite but unbounded lifetime. Finally, Type 3 bubbles occur when the discounted price is a strict local martingale, meaning its expectation strictly decreases over time. These type 3 bubbles are of central importance in this thesis, as they directly capture the strict local martingale behavior that allows market prices to exceed their fundamental values. Having established our no free lunch conditions and martingale methodology, we now examine how identities manifest from these in derivative markets.

1.2 Option theory for bubbles

Derivative securities provide an important insight for understanding bubbles, since they allow us to compare observed option prices with their theoretical fundamental values. If bubbles exist in the underlying asset they transmit into option markets in predictable ways Jarrow, Protter and Shimbo (2006). This makes option pricing identities such as put-call parity, useful in detecting and characterizing bubbles (Cox and Hobson, 2005). Throughout this section, we fix a valuation time t and write $C(K,T), P(K,T), F(K,T)$ for the observed prices of the call option, put option and forward respectively. We define the fundamental value of these derivatives as,

$$C^*(K,T) = \mathbb{E}_{\mathbb{Q}}[(S_T - K)^+], \tag{1.2.1}$$

$$P^*(K,T) = \mathbb{E}_{\mathbb{Q}}[(K - S_T)^+], \tag{1.2.2}$$

$$F^*(K,T) = C^*(K,T) - P^*(K,T) = \mathbb{E}_{\mathbb{Q}}[S_T] - K. \tag{1.2.3}$$

We assume that S pays no dividends and use general r when deriving the parity gap identity, then specialise to discounted prices ($r = 0$) for the recovery of formulas.

Before drawing inferences about bubbles from options, we separate value into two layers. The fundamental price which is its risk-neutral conditional expectation, and the observed price which is what the asset trades for in the market. In the classical arbitrage free framework these coincide, but in the presence of bubbles they can diverge. Put-Call parity is the easiest place to see what must hold at the fundamental level, and what still holds at market prices under the No-Dominance condition defined in Jarrow, Protter and Shimbo (2006). We define No Dominance as such,

Assumption 3 (No Dominance) For any stopping time σ, if

$$D^2_{\sigma+u} - D^2_\sigma \;\geq\; D^1_{\sigma+u} - D^1_\sigma \quad \text{and} \quad X^2_\tau \mathbf{1}_{\{\tau>\sigma\}} \;\geq\; X^1_\tau \mathbf{1}_{\{\tau>\sigma\}} \quad \text{for } u>0, \tag{1.6}$$

then $V^2_\sigma \geq V^1_\sigma$. Furthermore, if for some stopping time σ:

$$\mathbb{E}\Big[\mathbf{1}_{\{D^2_\infty - D^2_\sigma > D^1_\infty - D^1_\sigma\} \cup \{X^2_\tau \mathbf{1}_{\{\tau>\sigma\}} > X^1_\tau \mathbf{1}_{\{\tau>\sigma\}}\}} \;\Big|\; \mathcal{F}_\sigma\Big] > 0, \tag{1.7}$$

Having defined this we can now define the fundamental price of an option,

Definition 1.2.1. *(Fundamental price of an option) The fundamental price $V^*_t(H)$ of a European option with payoff H at maturity T is given by*

$$V^*_t(H) = \mathbb{E}_{\mathbb{Q}}[H(S_T)|\mathcal{F}_t], \tag{1.2.4}$$

where $H(S_T)$ denotes a functional of the path of S on the time interval [0,T].That is, $H(S_T) = H(S_r; 0 \leq r \leq T)$

Theorem 1.2.2. *(Put-Call Parity for Fundamental Prices)*

$$C^*_t(K) - P^*_t(K) = \mathbb{E}_{\mathbb{Q}}[S_T|\mathcal{F}_t] - K. \tag{1.2.5}$$

Proof. The proof follow from the linearity of conditional expectation. At maturity to

$$(S_T - K)^+ - (K - S_T)^+ = S_T - K, \qquad \forall K \geq 0. \tag{1.2.6}$$

Since the fundamental price of an option with payoff function H is $\mathbb{E}_{\mathbb{Q}}[H(S)_T|\mathcal{F}_t]$ we have

$$\begin{aligned} C^*_t(K) - P^*_t(K) &= \mathbb{E}_{\mathbb{Q}}[(S_T - K)^+|\mathcal{F}_t] - \mathbb{E}_{\mathbb{Q}}[(K - S_T)^+|\mathcal{F}_t], && (1.2.7)\\ &= \mathbb{E}_{\mathbb{Q}}[S_T - K|\mathcal{F}_t], && (1.2.8)\\ &= \mathbb{E}_{\mathbb{Q}}[S_T|\mathcal{F}_t] - K. && (1.2.9) \end{aligned}$$

□

By contrast, in markets with bubbles under no dominance conditions, put call parity for observed prices is defined as $C(K,T) - P(K,T) = S_t - K$. This asymmetry is important as

it allows puts to coincide with their fundamental value $P(K,T) = P^*(K,T)$, highlighting that puts options do not have bubbles, whereas calls differ by a non-negative bubble term. This identity provides the benchmark against which all observed prices will be read. It also highlights the quantity that will diagnose bubbles as if S is a strict local martingale under $\mathbb{Q}$ then its fundamental price will be less than the market price $\mathbb{E}_{\mathbb{Q}}[S_T|\mathcal{F}_t] < S_t$ Jarrow, Kchia and Protter (2011).

A single maturities option sheet contains far more than the linear relation above, because the shape of the call price across strikes encodes the entire risk neutral law of S_T. Following the identities used in Jarrow and Kwok (2021), we write $f_{S_T}(\cdot \mid \mathcal{F}_t)$ for its density when it exists. We start with the integral representation of the payoff,

$$(S_T - K)^+ = \int_{u=K}^{\infty} \mathbf{1}_{\{S_T \geq u\}} du. \tag{1.2.10}$$

Taking conditional expectations, we gain the fundamental value of a call option as an integral of tail probabilities,

$$C^*(K,T) = \mathbb{E}_{\mathbb{Q}}[(S_T - K)^+ \mid \mathcal{F}_t] = \int_K^{\infty} \mathbb{Q}(S_T \geq u \mid \mathcal{F}_t) du. \tag{1.2.11}$$

Writing $F(K) = \mathbb{Q}(S_T \leq K \mid \mathcal{F}_t)$ and differentiating in the strike (justified by dominated convergence) then gives, for almost every $K > 0$,

$$\frac{\partial C^*}{\partial K}(K,T) = -\mathbb{Q}(S_T \geq K \mid \mathcal{F}_t), \qquad \frac{\partial^2 C^*}{\partial K^2}(K,T) = -\frac{\partial}{\partial K}(1 - F(K)) = f_{S_T}(K \mid \mathcal{F}_t), \tag{1.2.12}$$

and equivalently for puts we get,

$$\frac{\partial P^*}{\partial K}(K,T) = \mathbb{Q}(S_T \leq K \mid \mathcal{F}_t), \qquad \frac{\partial^2 P^*}{\partial K^2}(K,T) = \frac{\partial}{\partial K} F(K) = f_{S_T}(K \mid \mathcal{F}_t). \tag{1.2.13}$$

Differentiation under the integral in (1.3.8) is justified by dominated convergence, since $\partial_K (x - K)^+ = -1_{\{x \geq K\}}$ and $|(S_T - K)^+| \leq S_T$ with $\mathbb{E}_{\mathbb{Q}}[S_T \mid \mathcal{F}_t] < \infty$. Hence for fixed $T, K \mapsto C^*(K,T)$ is decreasing and convex, and $\partial_K^2 C^*(K,T) = \partial_K^2 C^*(K,T) = f_{S_T}(K \mid \mathcal{F}_t)$, the conditional distribution of S_T is then recovered from a single call curve (Jarrow and Kwok, 2021).

Because observed prices are used in empirical work, it will be useful to us to connect these relations to the market setting in which put-call parity may fail. Following Jarrow and Kwok (2021), we write the parity gap as,

$$\Pi(K) = C(K,T) - P(K,T) - (S_t - e^{-rT}K). \tag{1.2.14}$$

Differentiating this with respect to K gives

$$\frac{d\Pi}{dK}(K) = \frac{dC}{dK}(K,T) - \frac{dP}{dK}(K,T) + e^{-rT}. \tag{1.2.15}$$

Using the put slope from (1.3.10), $\frac{dP}{dK} = e^{-rT}\mathbb{Q}(S_T \leq K \,|\, \mathcal{F}_t)$ and rearranging,

$$\frac{dC}{dK}(K,T) = -e^{-rT}\mathbb{Q}(S_T \geq K \,|\, \mathcal{F}_t) + \frac{d\Pi}{dK}. \tag{1.2.16}$$

Under the no dominance assumption we adopted for market prices, $\Pi \equiv 0$ and bounded European claims price at fundamental value. With discounted prices ($r = 0$) (1.2.14) reduces exactly to the fundamental slope identity in (1.2.12). Thus the distribution recovered from a smoothed call sheet is the fundamental distribution even when market data is used (Jarrow and Kwok, 2021).

The risk neutral mean of S_T is obtained from the same option sheet via a double integral argument. We start from the tail-integral representation for $x \geq 0$

$$x = \int_{y=0}^{\infty} \mathbf{1}_{\{x \geq y\}}\, dy. \tag{1.2.17}$$

Substituting $x = S_T$ and taking conditional expectations we get,

$$\mathbb{E}_{\mathbb{Q}}[S_T \,|\, \mathcal{F}_t] = \mathbb{E}_{\mathbb{Q}}[\int_0^{\infty} \mathbf{1}_{\{S_T \geq y\}}\, dy \,|\mathcal{F}_t\,] = \int_0^{\infty} \mathbb{E}_{\mathbb{Q}}[\mathbf{1}_{\{S_T \geq y\}} \,|\, \mathcal{F}_t]\, dy = \int_0^{\infty} \mathbb{Q}(S_T \geq y \,|\, \mathcal{F}_t)\, dy. \tag{1.2.18}$$

Equivalently, if a conditional density exists we have,

$$\mathbb{E}_{\mathbb{Q}}[S_T \,|\, \mathcal{F}_t] = \int_{x=0}^{\infty}\int_{y=0}^{\infty} \mathbf{1}_{\{x \geq y\}} f_{S_T}(x \,|\, \mathcal{F}_t)\, dy\, dx = \int_{y=0}^{\infty}\int_{x=y}^{\infty} f_{S_T}(x \,|\, \mathcal{F}_t)\, dx\, dy, \tag{1.2.19}$$

where we swapped the order of the non-negative integrand. Substituting the slope identity from (1.2.12) into (1.2.19) converts the outer integral into an integral of the call's strike slope,

$$\mathbb{E}_{\mathbb{Q}}[S_T \,|\, \mathcal{F}_t] = -\int_0^{\infty} \frac{\partial C^*}{\partial K}(K,T)\, dK. \tag{1.2.20}$$

Integrating by parts and taking upper and lower limits on K then gives the boundary,

$$\mathbb{E}_{\mathbb{Q}}[S_T|\mathcal{F}_t] = \lim_{K\downarrow 0} C^*(K,T) - \lim_{K\uparrow\infty} C^*(K,T). \tag{1.2.21}$$

As $K \downarrow 0, (S_T - K)^+ \uparrow S_T$ so $\lim_{K\downarrow 0} C^*(K,T) = \mathbb{E}_{\mathbb{Q}}[S_T \,|\, \mathcal{F}_t]$ (monotone convergence). As $K \uparrow \infty, (S_T - K)^+ \downarrow 0$ and $(S_T - K)^+ \leq S_T$ so $\lim_{K\uparrow\infty} C^*(K,T) = 0$ (dominated convergence). Hence $C^*(0,T) = \mathbb{E}_{\mathbb{Q}}[S_T \,|\, \mathcal{F}_t]$. When strikes are observed on a finite interval, the integral in (1.2.20) is evaluated over the quoted range and the tails are bounded using

the monotonicity and convexity implied by (1.2.11) - (1.2.12), this is exactly the partial-identification procedure in Jarrow and Kwok (2021). Biagini et al. (2024) showed that observed call's were equal to their fundamental price plus this additive, strike-independent constant, while European puts remains the same as their fundamental value,

Proposition 1.2.3. *For every K and T,*

$$C(K,T) = C^*(K,T) + m(T), \qquad P(K,T) = P^*(K,T). \tag{1.2.22}$$

This is exactly the pricing result in Biagini et al. (2024) (with collateral level $\alpha = 1$), and the upper and lower bounds of the call option becomes,

$$\lim_{K\downarrow 0} C(K,T) = S_t, \qquad \lim_{K\uparrow\infty} C(K,T) = m(T). \tag{1.2.23}$$

As $K \downarrow 0$ the put payoff $(K - S_T)^+ \to 0$ so $P \to 0$ and observed parity $C - P = S_t - K$ forces $\lim_{K\downarrow 0} C(K,T) = S_t$. As $K \uparrow \infty$, $C^*(K,T) \to 0$ by dominated convergence, hence $C(K,T) \to m(T)$ since $C = C^* + m(T)$. Combining the boundary identity with these deep-strike limits yields,

$$S_t = E_Q[S_T \,|\, \mathcal{F}_t] + m(T). \tag{1.2.24}$$

Because $m(T)$ is constant in K, the slope and curvature and hence the recovered price density are unaffected by the presence of a bubble. In implementation an arbitrage free call curve (non-negative, decreasing and convex in K) is fitted to each maturity. The identities above turn a single option sheet into three measurable objects, the risk neutral distribution, the conditional mean, and the bubble gap $m(T)$. In the next chapter we build upon these identities to prove the existence of stirct local martingales in princing models and apply them to detect bubbles in three complementary ways.

Chapter 2

Mathematical Models that do and don't bubble

To illustrate the concept of financial bubbles in a continuous time setting we examine several examples under the risk-neutral measure $\mathbb{Q}$. The following examples from the literature not only validate the theoretical constructs outlined earlier but also provide tangible models that capture the dynamics of speculative price inflation observed in real markets. For simplicity, if we assume that there are no dividend payments and the risk free rate $r = 0$, our bubble test then becomes,

$$\text{no bubble exists} \Leftrightarrow \mathbb{E}_{\mathbb{Q}}[S_T \,|\, \mathcal{F}_t] = S_0, \qquad \text{a bubble exists} \Leftrightarrow \mathbb{E}_{\mathbb{Q}}[S_T|\mathcal{F}_t] < S_0, \tag{2.0.1}$$

and we write $m(T) = S_0 - \mathbb{E}_{\mathbb{Q}}[S_T] \geq 0$ for the bubble gap.
We begin with the Black-Scholes model, demonstrating that in this setting the discounted stock price is a true martingale, so that on any finite time horizon $[0, T]$ we have $\mathbb{E}_{\mathbb{Q}}[S_T] = S_0$ and there is no bubble gap $m(T) = 0$. We then move onto the Constant-Elasticity-of-Variance (CEV) diffusion and demonstrate that this local volatility model has the possibility to produce a strict local martingale and in turn a bubble. Finally, as a stochastic volatility benchmark, we use the SABR model to demonstrate that a strict local martingale remains with the discounted stock price providing $m(T) > 0$ as expected. Additionally, we verify these models by introducing a Monte Carlo simulation, allowing us to ensure and quantify the bubble gap is non negative, when a bubble is present $m(T) > 0$.

2.1 Black-Scholes model

The Black-Scholes model is a fundamental cornerstone for option pricing as it is the first internally consistent framework that ties together no-arbitrage, dynamic replication and closed form valuation Black and Scholes (1973). In its risk neutral formulation, the stock price follows a geometric Brownian motion with constant volatility, which implies a complete market and a unique no-arbitrage price for any European claim. In practice, however,

these ideal assumptions rarely hold. Real markets are often incomplete and transient mis-pricing can appear, so the Black-Scholes assumptions are at best approximations (Jarrow, Protter and Shimbo, 2010). This gap between theory and reality invites scrutiny of the model's effectiveness, but remains fundamental due to its efficiency and simplicity.
We define the risk neutral dynamics of the stock price under the Black-Scholes model as follows,

$$dS_t = (r - d)S_t dt + \sigma S_t dW_t. \tag{2.1.1}$$

Where r is the risk-free rate d is the dividend payments, σ is the volatility, S_t is the underlying assets price, and W is a standard Brownian motion. Satisfying the usual assumption as in Black and Scholes (1973), where the risk free rate is zero, the underlying asset does not pay dividends, there are no transaction fees or taxes and the market is complete and arbitrage free, the solution is then,

$$S_t = S_0 \exp(\sigma W_t - \frac{1}{2}\sigma^2 t). \tag{2.1.2}$$

We now prove that under the Black-Scholes model does not account for bubbles as it is a true martingale.

Proposition 2.1.1. *The discounted price $\tilde{S}_t = e^{-rt}S_t$ is a true martingale under $\mathbb{Q}$. Equivalently, for all $T > 0$,*

$$\mathbb{E}_{\mathbb{Q}}[\tilde{S_T}] = \tilde{S_0} \quad \textit{and} \quad \mathbb{E}_{\mathbb{Q}}[S_T] = S_0 e^{rT}. \tag{2.1.3}$$

Hence the bubble gap $m(T) = \tilde{S_0} - \mathbb{E}_{\mathbb{Q}}[\tilde{S_T}]$ is identically 0, i.e. the Black-Scholes model cannot generate a strict local martingale (no bubble)

Proof. Under the discounted price $\tilde{S_t} = e^{-rt}S_t$ equations (2.1.1) and (2.1.2) respectively become,

$$d\tilde{S_t} = \sigma \tilde{S_t} dW_t, \qquad \tilde{S} = \tilde{S_0} \exp(\sigma W_t - \frac{1}{2}\sigma^2 t). \tag{2.1.4}$$

Since $W_T \sim N(0, T)$,

$$\mathbb{E}_{\mathbb{Q}}[\tilde{S_T}] = \tilde{S_0}\mathbb{E}_{\mathbb{Q}}[e^{\sigma W_T - \frac{1}{2}\sigma^2 T}] = \tilde{S_0} e^{\frac{1}{2}\sigma^2 T - \frac{1}{2}\sigma^2 T} = \tilde{S_0}. \tag{2.1.5}$$

Since $\tilde{S_0} = S_0$, $E_{\mathbb{Q}}[\tilde{S_T}] = \tilde{S_0}$ is equivalent to $E_{\mathbb{Q}}[S_T] = S_0 e^{rT}$. Hence $m(T) = \tilde{S_0} - \mathbb{E}_{\mathbb{Q}}[\tilde{S_T}] = \tilde{S_0} - \tilde{S_0} = 0$ □

One of the defining assumptions of Black-Scholes is that if priced under the risk neutral measure $\mathbb{Q}$, the underlying follows a geometric Brownian motion with constant volatility (Black and Scholes, 1973). If that were true, all European options on the same underlying asset would share a single volatility parameter, independent of strike and maturity, causing the entire volatility surface to be flat. Empirically this is not the case, as when market

prices are inverted through the Black-Scholes formula, the recovered implied volatility varies systematically with strike and maturity, producing expected volatility smile patterns (Dupire, 1994). Yan (2023) demonstrated this on the popular semiconductor index PHLX as shown in Figure 2.1. The presence of the volatility smile is a clear deviation from the Black-Scholes model assumptions, indicating that the constant volatility assumption is too restrictive for real markets, and motivates extensions such as local and stochastic volatility models.

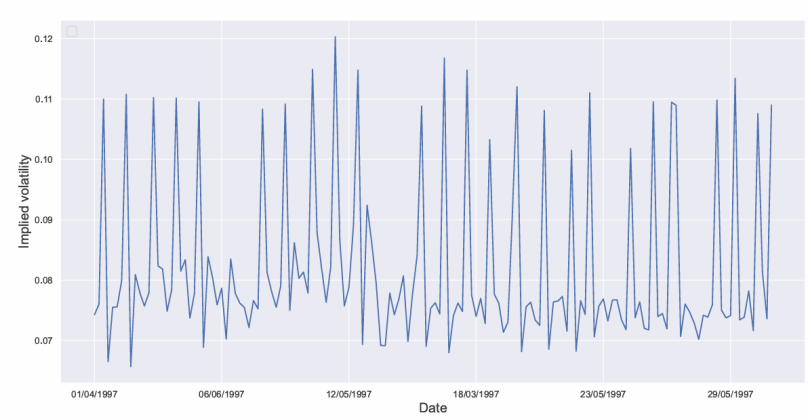

Figure 2.1: Implied volatility of PHLX Yan (2023).

As shown above in proposition 2.1.1, the Black-Scholes model under risk-neutral dynamics of the underlying asset is a global martingale. This is problematic as we know that from Definition 1.1.11 that financial bubbles only exist if S is a strict local martingale under the risk-neutral measure $\mathbb{Q}$. However, these limitations from the Black-Scholes have motivated the evolution of new models involving local and stochastic volatility rather than a constant volatility, as these better capture market observations such as the volatility smile. We investigate local and stochastic volatility models further namely the CEV and SABR models and demonstrate that under these models strict local martingales can be present and in turn a bubble.

2.2 Local volatility models

The local volatility model extends Black-Scholes by allowing volatility to depend on time and the current price of the asset, better replicating market dynamics. This model has two main advantages over Black-Scholes. Firstly, local volatility models can fit the entire cross-section of European option prices exactly, rather than forcing a single constant σ. This is extremely useful in replicating the volatility smile prevalent in markets. Using Dupire's formula, the local volatility model creates a bridge between the observed option surface and the underlying asset's dynamics, providing a more descriptive and interpretable account of the price evolution. Secondly, the model can generate option prices that account

for bubbles. By choosing the growth of $\sigma_{loc}(t,s)$ appropriately, the discounted price becomes a strict local martingale, unlike at-most-linear growth models that remain true martingales and exclude bubbles.

We define the risk neutral dynamics of the stock price under the local volatility model as,

$$dS_t = (r-d)S_t dt + \sigma_{loc}(S_t,t)S_t dW_t. \tag{2.2.1}$$

Where r is the risk free rate, q is the dividend yield, W_t is a Brownian motion, S_t is the underlying asset price and $\sigma(S_t,t)$ is the instantaneous volatility as a function of the underlying asset price and time. A vital deduction from the local volatility model is the Dupire formula, allowing us to recover the local volatility directly from option prices Dupire (1994).

Theorem 2.2.1. *(Dupire Formula). Let $C = C(K,T)$ be the price of a call option. The local volatiltiy σ satisfies,*

$$\sigma^2(T,K) = \frac{\frac{\partial C}{\partial T} + (r-d)K\frac{\partial C}{\partial K} + dC}{\frac{K^2}{2}\frac{\partial^2 C}{\partial K^2}}. \tag{2.2.2}$$

Proof. We follow Yan (2023)'s proof however alternative proofs can be found in Itkin (2020). We begin by letting $p(s,t)$ be the probability distribution function (PDF) of the stock price at time t and the stock price S_t. It satisfies the Kolmogorov forward equation,

$$-p_t - (r-d)(sp)_s + \frac{1}{2}(\sigma(t,s)s^2 p)_{ss} = 0,\ t > 0. \tag{2.2.3}$$

The initial condition is $p(s,0) = \delta_{S_0}(s)$. The price of the call option can then be wrote as,

$$C(K,T) - e^{-rT}\mathbb{E}_{\mathbb{Q}}[(S_T - K)^+] = e^{-rT}\int_K^\infty (s-K)\,p(s,T)ds. \tag{2.2.4}$$

Taking the partial derivative of $C(T,K)$ with respect to K, we get

$$C_K(T,K) = e^{-rT}\int_K^\infty -p(s,T)\,ds. \tag{2.2.5}$$

Then taking the partial derivative with respect to K again, we are left with

$$C_{KK}(T,K) = e^{-rT}p(s,T)\,ds. \tag{2.2.6}$$

Differentiating the price of the call option with respect to T yields,

$$C_T(K,T) = -rC(K,T) + e^{-rT}\int_K^\infty (s-K)p_T(s,T)ds. \tag{2.2.7}$$

Using the Forward Kolmogorov equation we are left with,

$$C_T = -rC + e^{-rT}\int_K^\infty (s-K)(r-d)(sp)_s\,ds + \frac{1}{2}r^{-rT}\int_K^\infty (s-K)(r-d)(\sigma^2 s^2 p)_{ss}\,ds. \quad (2.2.8)$$

Calculating integration parts, we get

$$C_T = -rC + e^{rT}(r-d)\int_K^\infty sp\,ds + \frac{1}{2}e^{-rT}\sigma^2 K^2 p, \quad (2.2.9)$$

rearranging this and using all previous results and $e^{-}rT\int_K^\infty spds = C - KC_K$ and $e^{-rT}p = C_{KK}$ we get the Dupire formula as in (2.2.2). □

Given a calibrated option surface, the call price $C(K,T)$ can be viewed as a smooth function of strike and maturity, and Dupire's formula recovers the local variance $\sigma^2_{loc}(K,T)$ from its partial derivatives. In practice this is a very delicate process, market quotes must first be fitted by an arbitrage-free surface (monotone in T, decreasing and convex in K), then smoothed so that $\partial_T C$ and $\partial_{KK} C$ are numerically stable **?**. Without such preprocessing, the extracted σ_{loc} can often be noisy and unreliable especially at extreme strikes and maturities. While Local volatility makes valuable adjustments to the Black-Scholes model there is still some limitation. Because $\sigma_{loc}(t,s)$ is deterministic, the model implies restricted dynamics, tends to understate the volatility of volatility, and its Greeks can be less robust to market moves than those from genuine stochastic volatility models. Despite these caveats, local volatility remains widely used, commonly for path-dependent and barrier options, precisely because it matches the current volatility smile across strike and maturities and is tractable for calibration and options pricing. The main advantage that local volatility has over the Black-Scholes model in our case, is that its discounted price can be a strict local martingale, generating a positive bubble gap $m(T) = S_0 - \mathbb{E}_{\mathbb{Q}}[S_T]$. This is often due to $\sigma_{loc}(t,s)$ growing faster in s at high levels. We demonstrate this result in a popular model known as the constant elasticity of variance (CEV) model where when $\beta > 1$ a bubble exists.

In the Black–Scholes model we established that an asset price process exhibits a bubble when, under the risk–neutral measure $\mathbb{Q}$, the discounted price is a strict local martingale rather than a true martingale. While this provides a rigorous theoretical definition, it does not immediately offer a viable criterion for detecting such behaviour within a given model with local or stochastic volatility. Feller's test provides exactly this, a practical condition to determine whether a diffusion process can reach infinity in finite time, which is directly linked to the presence of bubbles Delbaen and Shirakawa (2002); Mijatović and Urusov (2012).

Theorem 2.2.2. *(Feller's Test for Explosions) Consider an asset price process modelled*

by the Stochastic Differential Equation (SDE)

$$dS_t = \sigma(S_t)dW_t, \qquad S_0 > 0. \tag{2.2.10}$$

Where W_t is a Brownian motion and $\sigma(x) > 0$ is a measurable volatility function. Then the boundary at infinity is attainable in finite time if and only if,

$$\int_\epsilon^\infty \frac{x}{\sigma^2(x)}dx < \infty. \tag{2.2.11}$$

If condition (2.2.11) holds (the integral is finite) and hence the model admits a bubble, whereas if (2.2.11) fails , the integral diverges and bubbles are excluded. This gives a clear, tractable test for bubble behaviour in diffusion models. We now apply this Theorem to the Constant Elasticity of Variance (CEV) model to illustrate its implications and demonstrate that a strict local martingale exists. Under risk neutral dynamics the CEV model satisfies,

$$dS_t = (r-d)S_t dt + \sigma S_t^\beta dW_t \tag{2.2.12}$$

and define the discounted price as follows,

$$\tilde{S}_t = e^{-(r-d)t}S_t \iff S_t = e^{(r-d)t}\tilde{S}_t. \tag{2.2.13}$$

By Itô's formula

$$d\tilde{S}_t = \sigma e^{(\beta-1)(r-d)t}\tilde{S}_t^\beta dW_t, \qquad \tilde{S}_0 = S_0. \tag{2.2.14}$$

Thus $\tilde{S}$ is a non-negative local martingale with a deterministic time factor $a(t) = e^{(\beta-1)(r-d)t}$.

Theorem 2.2.3. *(CEV martingality). Fix any finite horizon $T > 0$. Then,*

$$\beta \leq 1 \Rightarrow \mathbb{E}_\mathbb{Q}[e^{-(r-d)T}S_T] = S_0, \quad \textit{(no bubble).} \tag{2.2.15}$$

$$\beta > 1 \Rightarrow \mathbb{E}_\mathbb{Q}[e^{-(r-d)T}S_T] < S_0, \quad \textit{(bubble).} \tag{2.2.16}$$

Equivalently in non discounted units,

$$\beta \leq 1 \Longrightarrow \mathbb{E}_\mathbb{Q}[S_T] = S_0 e^{(r-d)T}, \qquad \beta > 1 \Longrightarrow \mathbb{E}_\mathbb{Q}[S_T] < S_0 e^{(r-d)T}. \tag{2.2.17}$$

Proof. From (2.2.14) set,

$$u(t) = \int_0^t a(s)^2 ds = \int_0^t e^{2(\beta-1)(r-d)s}ds, \qquad \hat{W}_u = \int_0^{t(u)} a(s)dW_s. \tag{2.2.18}$$

By Dambis-Dubins-Schwarz, $\hat{W}$ is a Brownian motion in the new time u. Writing $X_u = \tilde{S}_{t(u)}$ (2.2.14) becomes the time homogenous diffusion,

$$dX_u = \sigma X_u^{\beta} d\hat{W}_u, \qquad X_0 = S_0. \tag{2.2.19}$$

We can now apply Feller's test for explosions as in Theorem 2.2.2, allowing us to test the marginality of the driftless one-dimensional diffusion $dX = \sigma(X)dW$. Here we have that $\sigma(x) = \sigma x^{\beta}$ so,

$$\int^{\infty} \frac{x}{(\sigma x^{\beta})^2} dx = \frac{1}{\sigma^2} \int^{\infty} x^{1-2\beta} dx = \begin{cases} \infty & \beta \leq 1 \\ < \infty & \beta > 1 \end{cases} \tag{2.2.20}$$

hence X (and therefore $\tilde{S}$ is a true martingale if $\beta \leq 1$, and a strict local martingale if $\beta > 1$. Thus

$$\mathbb{E}_{\mathbb{Q}}[\tilde{S}_T] = S_0 \text{ for } (\beta \leq 1), \qquad \mathbb{E}_{\mathbb{Q}}[\tilde{S}_T] < S_0 \text{ for } (\beta > 1). \tag{2.2.21}$$

Multiplying by $e^{(r-d)T}$ gives the stated expectations for S_T (Dupire, 1994). □

From this we can then define the CEV bubble gap as $m(T) = S_0 - \mathbb{E}_{\mathbb{Q}}[e^{-(r-d)T} S_T] \geq 0$ when there exists a bubble and $m(t) = 0$ when bubbles are absent. This means that when $\beta > 1$ we should see that there is a positive bubble gap implying the existence of a bubble.

2.3 Stochastic volatility model - SABR

The Stochastic volatility model is another extension to the Black-Scholes model, introduced by Hull and White in the 1980's Hull and White (1987). Stochastic volatility is different to local volatility models in the sense that their volatility is no longer a fixed parameter based on the asset price and time but a stochastic process, introducing randomness into the volatility. This randomness comes in two form, one for the underlying asset and another for the volatility. We can represent the volatility σ_t of the underlying S_t as a function $\sigma(Y_t)$, where Y_t is an auxiliary process. Typically Y_t is characterised as a diffusion as we see below,

$$dS_t = (r-d)S_t dt + \sigma(Y_t) S_t dW_t^{(1)} \tag{2.3.1}$$

$$dY_t = \mu(Y_t)dt + \eta(Y_t) dW_t^{(2)} \tag{2.3.2}$$

$$d\langle W^{(1)}, W^{(2)} \rangle = \rho \, dt \tag{2.3.3}$$

where η and μ are its mean reversion and volatility of volatility, $W_t^{(1)}, W_t^{(2)}$ are two Brownian motions, and ρ is its correlation. Typically ρ is negative to incorporate the relative

that stock prices often go down when the volatility increases. This is a phenomenon known as the leverage effect. This framework keeps the one-factor price diffusion for S but enriches volatility smiles and dynamics through parameters (μ, η, ρ) (Hull and White, 1987). Stochastic volatility smiles and their dynamics allows non-trivial forward smiles, and provide a realistic description of clustering and mean reversion in volatility. The trade off's however are market incompleteness impacting the ability to perfectly hedge volatility risk, more parameters to calibrate, and heavier numerics for pricing and computing the Greeks. However, like local volatility models, stochastic volatility models have the opportunity to produce strict local martingales, an empirical feature for the detection of asset bubbles.
A popular stochastic volatility model is known as the SABR model proposed by Hagan, Lesniewski and Woodward (2015). The dynamics of the spot S and instantaneous volatility σ_t under the risk neutral measure for this model are specified as,

$$dS_t = (r-d)S_t dt + \sigma_t S_t^{\beta} dW_t^{(1)}, \qquad S_0 > 0 \tag{2.3.4}$$

$$d\sigma_t = \alpha \sigma_t dW_t^{(2)}, \qquad \sigma_0 > 0 \tag{2.3.5}$$

$$d\langle W^{(1)}, W^{(2)} \rangle_t = \rho \, dt, \qquad \alpha > 0 \tag{2.3.6}$$

If we are working with the discounted price $\tilde{S}_t = e^{-(r-d)t} S_t$ then we get,

$$d\tilde{S}_t = \sigma_t \tilde{S}_t^{\beta} e^{(\beta-1)(r-d)t} dW_t^{(1)} \tag{2.3.7}$$

Equivalently, for the maturity T forward $F_t = S_t e^{-(r-d)(T-t)}$ under its forward measure,

$$dF_t = \sigma_t F_t^{\beta} dW_t^{(1)} \tag{2.3.8}$$

$$d\sigma_t = \alpha \sigma_t dW_t^{(2)} \tag{2.3.9}$$

$$d\langle W^{(1)}, W^{(2)} \rangle_t = \rho \, dt \tag{2.3.10}$$

Setting $\beta = 0$ gives the standard SABR case The forward then evolves additively as $dF_t = \sigma_t dW_t^{(1)}$ so its increments are Gaussian. This specification admits simple formulas for call prices, but it allows F_t to become negative, which is not allowed for asset prices. Therefore we do not study the case where $\beta = 0$ but instead look at what happens when $\beta = 1$. When $\beta = 1$ the price is log-normal conditional on σ, and strict local martingales are able to exist. We demonstrate and prove this result below, showing that bubbles can exist in the SABR model when $\beta = 1$ (Hagan, Lesniewski and Woodward, 2015).

Theorem 2.3.1. *Let $\tilde{S}_t = e^{-(r-d)t} S_t$ in the model above with $\beta = 1$. Then for any finite*

$T > 0$,

$$\rho \leq 0 \Longrightarrow \mathbb{E}_{\mathbb{Q}}[\tilde{S_T}] = S_0, \qquad (\textit{true martingale}). \tag{2.3.11}$$

$$\rho > 0 \Longrightarrow \mathbb{E}_{\mathbb{Q}}[\tilde{S}_T] < S_0, \qquad (\textit{strict local martingale}). \tag{2.3.12}$$

Proof. We begin with the decomposition of the correlation,

$$W^{(1)} = \rho W^{(2)} + \sqrt{1-\rho^2} W^{\perp}, \tag{2.3.13}$$

where $W^{\perp}$ is a Brownian motion independent of $W^{(2)}$. Then,

$$M_t = \rho \int_0^t \sigma_s dW_s^{(2)} + \sqrt{1-\rho^2} \int_0^t \sigma_s dW_s^{\perp}. \tag{2.3.14}$$

Let,

$$R_t = \mathcal{E}(-\int_0^t \sqrt{1-\rho^2}\sigma_s \, dW_s^{\perp}). \tag{2.3.15}$$

For each fixed T, R_T is an integrable density.On any finite T, R_T is a true martingale and hence $\hat{\mathbb{Q}}$ is well defined and ε is the Doleáns-Dade stochastic exponential (Hagan, Lesniewski and Woodward, 2015; Mijatović and Urusov, 2012). By Girsanov, under the new measure Q, the process $W^{(2)}$ remains a Brownian motion and we have,

$$\mathbb{E}_{\mathbb{Q}}[\tilde{S}_T] = S_0 \, \mathbb{E}[\mathcal{E}(\int_0^T \rho\sigma_s dW_s^{(2)})]. \tag{2.3.16}$$

Hence the problem reduces to the stochastic exponential

$$Z_T = \mathcal{E}(\int_0^T \rho\sigma_s dW_s^{(2)}), \tag{2.3.17}$$

and either $E[Z_T] = 1$ (true martingale) or $E[Z_T] < 1$ (strict local martingale). If we let $X_t = \log \sigma_t$. Then from $d\sigma_t = \alpha\sigma_t dW_t^{(2)}$ we get,

$$dX_t = -\frac{1}{2}\alpha^2 dt + \alpha dW_t^{(2)}, \tag{2.3.18}$$

so X is a Brownian motion with drift. The integrand can then be written as

$$\rho\sigma_t = \rho e^{X_t} = b(X_t). \tag{2.3.19}$$

Thus,

$$Z_t = \mathcal{E}(\int_0^t b(X_s) dW_S^{(2)}). \tag{2.3.20}$$

Theorem 2.3.2 is utilised here from Mijatović and Urusov (2012) and states,

Theorem 2.3.2. *Let X solve $dX_t = \mu(X_t)dt + \sigma(X_t)dW_t$ on an interval (l, r). For*

$Z_t = \mathcal{E}(\int_0^t b(X_s)dW_s)$. *$Z$ is a true martingale on $[0,T]$ if and only if the auxiliary diffusion,*

$$d\tilde{X}_t = (\mu + \sigma^2 b)(\tilde{X}_t)dt + \sigma(\tilde{X}_t)dW_t, \tag{2.3.21}$$

is non-explosive at the boundary that corresponds to r, with boundary classification determined by the associated scale and speed measures.

In our case, $\mu(x) = -\frac{1}{2}\alpha^2, \sigma(x) = \alpha$ and $b(x) = \rho e^x$. Therefore the auxiliary drift is

$$\tilde{\mu}(x) = \mu(x) + \sigma(x)^2 b(x) = -\frac{1}{2}\alpha^2 + \alpha^2 \rho e^x. \tag{2.3.22}$$

The state space is $\mathbb{R}$ (since $\sigma_t > 0$ and $X_t = \log\sigma_t$). We must examine the right boundary ∞, the left boundary $-\infty$ need not be examined. computing the scale density p and speed density m for $\tilde{X}$,

$$p(x) = \exp(-\int^x \frac{2\tilde{\mu}(y)}{\sigma(y)^2}dy) = \exp(-\int^x (-1 + 2\rho e^y)\, dy) = exp(x - 2\rho e^x), \tag{2.3.23}$$

$$m(x) = \frac{2}{\sigma(x)^2 p(x)} = \frac{2}{\alpha^2} e^{-x+2\rho e^x}. \tag{2.3.24}$$

Let $s(x) = \int^x p(y)\, dy$ be the scale function. Applying the Feller's test we then get two cases,

Case : $\rho \leq 0$.

For large y, $p(y) = e^{y-2\rho e^y} \geq e^y$ hence,

$$s(+\infty) = \int^{+\infty} p(y)dy = \infty. \tag{2.3.25}$$

The boundary $+\infty$ is not attainable, the auxiliary diffusion is non-explosive, and by the criterion Z is a true martingale on any finite horizon. $E_Q[Z_T] = 1$, hence $E[\tilde{S_T}] = S_0$

Case : $\rho > 0$.

For large y, $p(y) = e^{y-2\rho e^y}$ decays so fast that,

$$s(+\infty) = \int^{+\infty} p(y)dy = \int^{+\infty} e^{y-2\rho e^y}dy = \int^{+\infty} e^{-2\rho u}du, \qquad (u = e^y) = \frac{1}{2\rho} < \infty. \tag{2.3.26}$$

Moreover,

$$s(+\infty) - s(y) = \int_y^{+\infty} p(z)dz = \int_{e^y}^{+\infty} e^{-2\rho u}\frac{du}{u} \sim \frac{e^{-2\rho e^y}}{2\rho e^y}, \qquad (y \to +\infty), \tag{2.3.27}$$

$$(s(+\infty) - s(y))m(y) \sim \frac{1}{\alpha^2\rho}e^{-y} \qquad (y \to +\infty) \tag{2.3.28}$$

which is integrable at $+\infty$. With $s(+\infty) < \infty$, the boundary $+\infty$ is explosive for $\tilde{X}$, the criterion then yields that Z is a strict local martingale on any interval $[0,T]$, hence a

bubble can exist by definition. Consequently $E[Z_T] < 1$ and $E[\tilde{S}_T] < S_0$ □

We have now established if bubbles can arise in the Black-Scholes model, local volatility model CEV, and stochastic volatility model SABR and under which conditions for the model needs for bubbles to arise. In the next section we move from showing that bubbles can exist to measuring and quantifying this bubbles component via the strike-independent gap defined in (1.2.3). We also demonstrate the convergence at the far out-the-money call tail.

Chapter 3

Modelling of the bubble gap $m(T)$

From Section 1.2, in discounted units the observed call satisfies,

$$C(K,T) = C^*(K,T) + m(T), \qquad \lim_{K\uparrow\infty} C(K,T) = m(T). \tag{3.0.1}$$

while puts coincide with their fundamental value, so bubbles do not appear in put prices. In this section, we practically demonstrate the fundamental identities of bubbles, utilising the models from Chapter 2 and real market data in the form of Nvidia options data. Using the identity of $m(T)$, we introduce complementary methods to display the behaviour of (3.0.1) and document the behaviour of these tools in the three models we defined earlier in this chapter, Black-Scholes, CEV, and SABR. Building upon these tests further, we then introduce an intuitive way to estimate the call tail and implement this on the real market. The aim of this section is to move from the existence of bubbles to a measurement of the bubble gap from a finite call sheet, allowing us to produce a method applicable to real market data.

3.1 Testing $m(T)$ with simulated data

For the tests implemented in this section we work in discounted units with $r = d = 0$ and a fixed maturity T. By Def.**??** we know that the bubble gap exists as,

$$m(T) = S_0 - \mathbb{E}_{\mathbb{Q}}[S_T] \geq 0. \tag{3.1.1}$$

This bubble gap vanishes if and only if the discounted price is a true martingale on $[0,T]$. From Section 1.2, we know that $m(T)$ is strike independent and as such, appears as a flat plateau at the far out-the-money end of the call. We wish to implement a method by which we can estimate $m(T)$ and demonstrate consequent properties of (3.0.1). First, we simulate multiple paths on the pricing process S_T and take the mean of this to give a Monte-Carlo estimate for S_T. We define this estimate as follows,

Definition 3.1.1. *(Monte-Carlo estimate). Given i.i.d. realisations of* $S_T^{(1)}, \dots, S_T^{(n)}$ *define,*

$$\widehat{m}_{mean}(T) = S_0 - \hat{S}_T, \qquad \hat{S}_T = \frac{1}{n}\sum_{i=1}^{n} S_T^{(i)}. \tag{3.1.2}$$

If $\mathbb{E}[|S_T|] < \infty$*, then by the strong law of large numbers,* $\widehat{m}_{mean}(T) \to m(T)$ *almost surely.*

This estimator is extremely attractive because it is numerically simple and directly reflects the properties of a strict local martingale. When a bubble is present, the Monte-Carlo sample mean converges to a value strictly below S_0. Moreover, because a non-negative local martingale is a supermartingale, $m(T) = S_0 - \mathbb{E}_Q[S_T]$ is non decreasing in T and typically increases. However, it is only used in simulation as a form of benchmarking.

In simulation we first compute the fundamental $C^*(K,T)$ from paths and then form a synthetic observed sheet $C_{obs} = C^* + \widehat{m}_{mean}$ to display the plateau. On market data we would apply the estimator directly to quotes. Assuming $\mathbb{E}[|S_T|] < \infty$ since $C^*(K,T) = \mathbb{E}_{\mathbb{Q}}[(S_T - K)^+]$, its right tail vanishes as $\lim_{K\to\infty} C^*(K,T) = 0$. Fixing a maturity T and observed call quotes $C_j = C(K_j, T)$ for $j = 1, \dots, n$, we fit an arbitrage-free call curve by projecting onto the cone of functions that are decreasing and convex in strike. On a general grid, with slopes $s_j := (y_{j+1} - y_j)/(K_{j+1} - K_j)$ and $K_1 < \cdots < K_n$, we solve the convex least-squares problem

$$\min_{y\in\mathbb{R}^n} \sum_{j=1}^{n} (C_j - y_j)^2 \quad \text{s.t.} \quad s_1 \le s_2 \le \cdots \le s_{n-1} \le 0,$$

which yields fitted values $C_{\text{obs}}^{\text{fit}}(K_j, T)$. This projection is implemented via isotonic regression (PAVA) on the slope vector $(s_j)_{j=1}^{n-1}$, followed by clipping $s_j \in [0,1]$ to enforce no-arbitrage bounds.

Because $K \mapsto C^*(K,T)$ is decreasing, convex, and has a zero right tail, the far-OTM part of the fitted fundamental curve is numerically flat near 0. We therefore use the average of the largest $m = \lceil 0.2\, n \rceil$ strikes as a diagnostic of the vanishing tail:

$$\widehat{L}_{\text{tail}} := \frac{1}{m} \sum_{j=n-m+1}^{n} C_*^{\text{fit}}(K_j, T) \;\approx\; \lim_{K\to\infty} C^*(K,T) \;=\; 0. \tag{3.1.3}$$

This is used as a sanity check for $C^*(K,T)$, not an estimator for $m(T)$. Here C_*^{fit} denotes the decreasing–convex fit to C^*. In market data (or for synthetic observed sheets in simulation, $C_{\text{obs}} := C^* + \widehat{m}_{\text{mean}}$) the analogous tail average recovers the bubble gap,

$$\widehat{m}_{\text{tail}} := \frac{1}{m} \sum_{j=n-m+1}^{n} C_{\text{obs}}^{\text{fit}}(K_j, T) \;\approx\; \lim_{K\to\infty} C(K,T) \;=\; m(T). \tag{3.1.4}$$

Now we turn to a bubble decision rule we adopt from the one-sided, finite-sample hypothesis test,

$$H_0 : m(T) = 0, \qquad H_1 : m(T) > 0. \tag{3.1.5}$$

Here, H_0 is the null hypothesis that there is no bubble gap and H_1 is the alternative hypothesis there is positive bubble gap. This test is built around the mean-shortfall route because it yields an explicit sampling distribution under resampling also known as bootstrapping. We apply this test only when i.i.d. draws of S_T are available (normally from path simulation). On raw market quotes, S_T is not observed, so we use only the tail-based estimator applied to the observed call surface. After projecting quotes (in discounted units) onto the decreasing-convex cone, we estimate $m(T)$ as the average of the far out-of-the-money fitted values; by $C = C^* + m(T)$, the right-tail limit equals $m(T)$. We resample the set of terminal prices $\{S_T^{(i)}\}_{i=1}^N$ with replacement to generate various "bootstrap experiments". Each bootstrap sample produces a bootstrap mean $\bar{S}_T^*$. The upper $(1-\alpha)$ quantile of these bootstrap means denoted by $Q_{1-\alpha}(\bar{S}_T^*)$ is then converted into a one-sided lower confidence bound for $m(T)$ by $m_{LB} = S_0 - Q_{1-\alpha}(\bar{S}_T^*)$. If $m_{LB} > 0$, we can reject H_0 at level α. Alongside this bound we report a one-sided bootstrapped p-value, defined as the empirical fraction of bootstrapped means that are at least S_0. The one-sided bootstrap p-value is $\hat{p} = \frac{1}{B}\sum_{b=1}^{B} \mathbf{1}\{\bar{S}_T^{*,b} \geq S_0\}$, where B is the number of bootstrap resamples. This procedure avoids parametric normality assumptions, has good coverage properties for sample means, and is straightforward to implement in simulation. On market data, we simply bootstrap the tail estimator by resampling quotes and refitting the curve.

These two methods serve different but complementary purposes in simulation. The mean-shortfall estimator and the associated bootstrap test provide a finite sample decision with a clear interpretation of how far the risk neutral mean sits below the spot price, and whether that shortfall is larger than can be explained by sampling noise. The tail-based estimator however, provides a model-free cross-check linked directly to the observed call surface. Therefore, if the bubble interpretation is correct, the fitted call curve will display a flat limit whose level equals the bubble gap. We demonstrate this in the experiments below, presenting both $\widehat{m}_{\text{mean}}(T)$ and $\widehat{m}_{\text{tail}}(T)$ and verifying that they agree in all three models as in Chapter 2. If these estimate methods agree, we will have strong evidence that the detected gap is not due to variations in a particular simulation scheme and that strike independence can be witnessed in practice.

3.2 Implementation of tests on synthetic data

We first begin our tests by quantifying the bubble gap $m(T) = S_0 - \mathbb{E}_{\mathbb{Q}}[S_T]$ at a single maturity $T = 1$ for the three models introduced earlier in Chapter 2, the Black-Scholes,

CEV with $\beta > 1$, and SABR with $\beta = 1$ and $\rho > 0$. This first look enables us to establish the qualitative pattern that should exist from the theory. Black-Scholes displays no bubble gap, while CEV ($\beta > 1$) and SABR ($\beta = 1, \rho > 0$) can exhibit a bubble gap under our parameter choices

All experiments are implemented in Python using a modular pipeline consisting of a simulator that returns discounted S_T samples, a one-sided bootstrap test of $m(T) > 0$, and a decreasing–convex call-curve fit via isotonic regression to recover the far-OTM tail. Because the testing logic depends only on simulated S_T (and, for the tail route, on a call sheet), the same code applies verbatim to other continuous-path models (e.g., Heston or local-volatility) by swapping in an alternative function. It can also be run on market data by skipping the simulator and feeding observed calls into the tail estimator, allowing this code can be utilised for future experimentation.

3.2.1 Sampling simulators

In order to run our tests we require i.i.d. draws of the discounted terminal price S_T at a fixed maturity and a call sheet, we use the models defined in Chapter 2 to do this. These samples feed directly into the model-free estimators we defined in Section 3.1. Throughout we work on a filtered probability space under the risk neutral measure $\mathbb{Q}$, with Brownian motions $W^{(1)}$, $W^{(2)}$ satisfying $d\langle W^{(1)}, W^{(2)}\rangle_t = \rho\, dt$. Integrands are predictable and square-integrable so the itô integrals we use are well-defined, and the Itô isometry

$$\mathbb{E}_{\mathbb{Q}}\left[\left(\int_0^T H_t dW_t\right)^2\right] = \mathbb{E}_{\mathbb{Q}}\left[\int_0^T H_t^2 dt\right]$$

holds. We will set ($r = d = 0$) in our experiments but write the sampling methods with r, d for demonstration purposes. We present the three separate sampling methods below.

Black-Scholes sampling

In discounted units the Stochastic Differential Equation (SDE) for the Black-Scholes model is $dS_t = \sigma S_t dW_t$. The solution to this is,

$$S_T = S_0 \exp(\sigma W_T - \frac{1}{2}\sigma^2 T),$$

so we can sample exactly by drawing $W_T \sim N(0, T)$, i.e. $S_T = S_0 \exp(\sigma\sqrt{T}Z - \frac{1}{2}\sigma^2 T)$ with $Z \sim N(0, 1)$. Since in discounted units $\mathbb{E}_{\mathbb{Q}}[S_T] = S_0$, the Black-Scholes can be seen as the control case as a bubble cannot exist (more details are provided in appendix A.0.1).

CEV sampling ($\beta > 1$)

From (2.2.14) the discounted CEV dynamics are,

$$d\tilde{S}_t = \sigma e^{(\beta-1)(r-d)t}\tilde{S}_t^{\beta} dW_t.$$

Sampling by the Lamperti power transform and setting $Y_t = \tilde{S}_t^{-(\beta-1)}$ as in Øksendal (2003), using Itó's formula gives,

$$dY_t = -(\beta-1)\sigma e^{(\beta-1)(r-d)t} dW_t + \frac{1}{2}(\beta-1)\beta\sigma^2 e^{2(\beta-1)(r-d)t} Y_t^{-1} dt.$$

We then apply the Euler-Maruyama scheme with a standard taming of the singular drift Y^{-1} to preserve positivity and numerical stability Sabanis (2016). On a grid $t_k = k\Delta t\,(\Delta t = T/M)$ we take one Euler step with $\Delta W_k = \sqrt{\Delta t} Z_k, Z_k \sim N(0,1)$,

$$Y_{k+1} = Y_k - (\beta-1)\sigma\Delta W_k + \frac{\frac{1}{2}(\beta-1)\beta\sigma^2\Delta t}{\max(Y_k, \varepsilon)}, \qquad \tilde{S}_{k+1} = Y_{k+1}^{-1/(\beta-1)}.$$

Since we are working in discounted units ($r = d = 0$), $\tilde{S}_{k+1} = S_{k+1}$ The small floor $\varepsilon > 0$ ensures $Y_k > 0$, and we clip extreme values of S_{k+1}.

SABR sampling ($\beta = 1$)

Under the T-forward measure (2.3.8 - 2.3.10),

$$dF_t = \sigma_t F_t dW_t^{(1)} \quad , d\sigma_t = \alpha\sigma_t dW_t^{(2)} \quad , d\langle W^{(1)}, W^{(2)}\rangle_t = \rho\, dt.$$

Solving the volatility SDE gives $\log\sigma_t = \log\sigma_0 - \frac{1}{2}\alpha^2 t + \alpha W_t^{(2)}$ and by Itó's formula,

$$\int_0^T \sigma_t dW_t^{(2)} = \frac{\sigma_T - \sigma_0}{\alpha}, \tag{3.2.1}$$

holds (Øksendal, 2003). From 2.3.13 we gain the decomposition $dW_t^{(1)} = \rho dW_t^{(2)} + \sqrt{1-\rho^2} dW_t^{\perp}$ where $W^{\perp}$ is a Brownian motion independent of $W^{(2)}$. Defining the integrated variance as $A_T := \int_0^T \sigma_t^2\, dt$, by Itô isometry we have,

$$J := \int_0^T \sigma_t\, dW_t^{\perp} \;\Big|\; \{\sigma_s\}_{0\le s\le T} \sim \mathcal{N}(0, A_T).$$

Combining (3.2.1) with the decomposition yields

$$\log\frac{F_T}{F_0} = \rho\,\frac{\sigma_T - \sigma_0}{\alpha} + \sqrt{1-\rho^2}\, J - \frac{1}{2}A_T, \qquad J \,|\, A_T \sim \mathcal{N}(0, A_T).$$

Since, in discounted units $F_T = S_T$ (and $F_0 = S_0$), this is the terminal distribution of the spot (Øksendal, 2003).

Generation of the call sheet

For a fixed maturity T, we first simulate i.i.d discounted prices $S_T^{(1)}, \ldots, S_T^{(N)}$ from a chosen model (GBM/CEV/SABR). We then choose a strike grid $K_1 < \cdots < K_n$ (typically on the range $0.1S_0 - 3S_0$). For each strike we then compute the discounted call by Monte-Carlo,

$$C(K_j, T) = \frac{1}{N} \sum_{i=1}^{N} (S_T^{(i)} - K_j)^+, \qquad j = 1, \ldots, m. \tag{3.2.2}$$

The collection $\{(K_j, C(K_j, T))\}_{j=1}^m$ is then the single-maturity call sheet that we can use for estimating the $\widehat{m}_{\text{tail}}(T)$. With market quotes the call sheet is given, so this step is omitted.

3.2.2 Results of test

For our tests we work in discounted units ($r = d = 0$) with $S_0 = 100$, $T = 1$, $B = 600$ in all simulations unless specified otherwise. For Figure 3.1 we simulated $N = 30000$ i.i.d. paths with $M = 1500$ time steps. The model specific parameters are as follows: for Black-Scholes $\sigma = 0.20$, for CEV $\beta = 1.5$, $\sigma = 0.16$, and for SABR $\beta = 1$, initial volatility $\sigma_0 = 0.25$, volatility of volatility $\nu = 2$ and correlation $\rho = 0.7$.

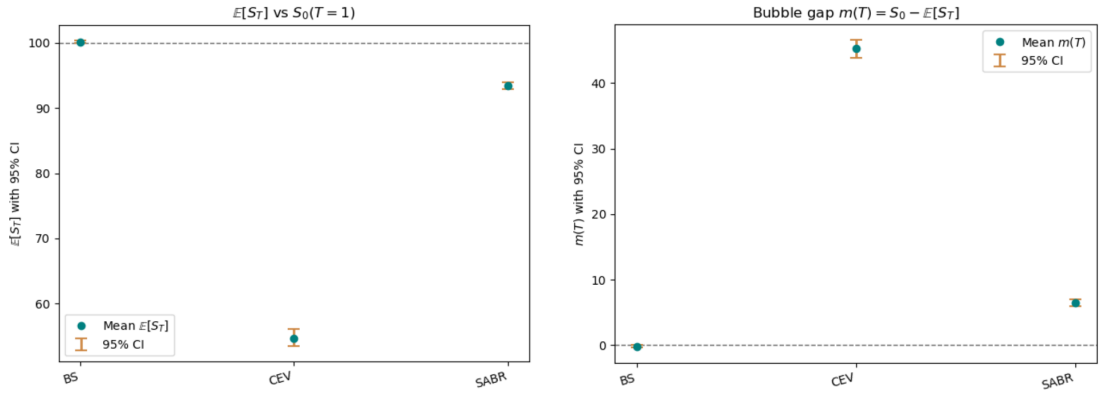

Figure 3.1: Risk neutral mean (left) and bubble gap $m(T) = S_0 - \widehat{\mathbb{E}_{\mathbb{Q}}}[S_T]$ (right) at $T = 1$. Error bars: two-sided 95% percentile-bootstrap intervals ($B = 600$). Black–Scholes is consistent with $m(T) = 0$; CEV ($\beta > 1$) and SABR ($\beta = 1, \rho > 0$) exhibit strictly positive gaps.

Table 3.1: One sided test of $H_0 : m(T) = 0$ at $T = 1$ (percentile bootstrap). m_{LB} is the one sided 95% lower bound for $m(T)$ (reject H_0 if $m_{\text{LB}} > 0$). The last column reports the descriptive two sided 95% CI for $m(T)$.

Model	$\widehat{\mathbb{E}}[S_T]$	$\widehat{m}_{\text{mean}}(T)$	$\widehat{m}_{\text{tail}}(T)$	m_{LB}	p-value	$m(T)$ 95% CI
Black-Scholes	100.166	-0.166	0	-0.374	0.935	$(-0.398,\ 0.054)$
CEV	54.713	45.287	50.492	44.802	0.000	$(43.865,\ 46.568)$
SABR	93.459	6.541	7.688	6.112	0.000	$(6.004,\ 7.028)$

From Figure 3.1 and Table 3.1 we can see that our results from these tests are extremely supportive of theory in Chapter 2. In the Black-Scholes model, the risk neutral mean sits essentially on the spot price, with $\widehat{\mathbb{E}}_{\mathbb{Q}}[S_T] \approx 100$ and $\widehat{m}(T) \approx 0$. The descriptive two sided 95% interval for the bubble gap $(-0.398, -0.054)$ is close to zero, and the one sided test delivers a negative lower bound $m_{\text{LB}} = -0.374$ with $p = 0.935$. The small negative estimate $\hat{m}(T) = S_0 - \widehat{\mathbb{E}}_{\mathbb{Q}}[S_T]$ observed in Table 3.1 is attributable to Monte-Carlo sampling variability, so there is no evidence to reject the hypothesis $H_0 : m(T) = 0$ and therefore the Black-Scholes model does not have a bubble. By contrast, in the CEV ($\beta = 1.5$) model the risk–neutral mean falls far below spot, $\widehat{\mathbb{E}}[S_T] \approx 54.713$, implying a large gap $\widehat{m}(T) = 45.287$ with a tight descriptive confidence interval (43.865, 46.568). The one sided bound is strongly positive, $m_{\text{LB}} = 44.802$ and $p = 0$, so we are able to reject the null decisively in favour of the alternative hypothesis $H_1 : m(T) > 0$ suggesting that a bubble may exist. The SABR ($\beta = 1, \rho = 0.7$) model shows a much milder but still meaningful effect with $\widehat{\mathbb{E}}_{\mathbb{Q}}[S_T] \approx 93.459$, $\widehat{m}(T) = 6.541$, a descriptive interval (6.004, 7.028), and a strictly positive lower bound $m_{\text{LB}} = 6.112$ with $p = 0$. These results are precisely in line with what is expected from the martingale theory in Chapter 2 imply, suggesting that our method implemented for detecting the bubble gap $m(T)$ is strongly reliable in these model settings.

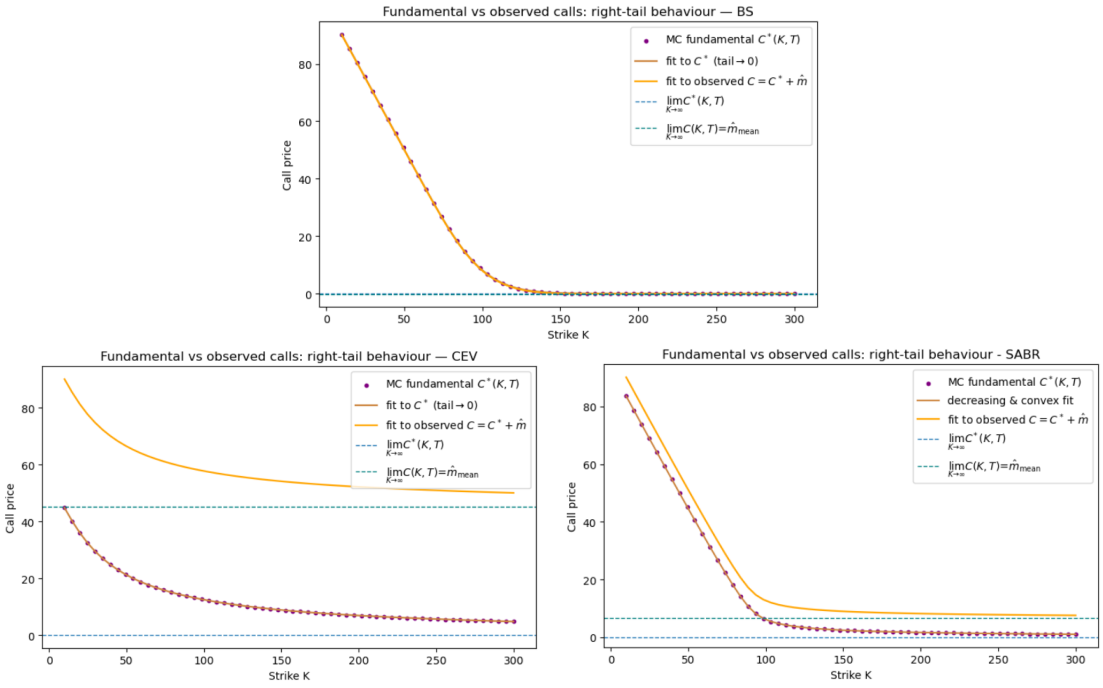

Figure 3.2: Right tail behaviour of call prices in discounted units ($T = 1$). Markers show Monte-Carlo fundamental calls $C^*(K,T)$ showing a decreasing-convex fit to C^* (with $\lim_{K\to\infty} C^*(K,T) = 0$). The orange solid line is the fitted "observed" call $C = C^* + \widehat{m}_{\text{mean}}$. Dashed horizontals mark the limiting levels, 0 for C^* and $\widehat{m}_{\text{mean}}$ for C. Top: Black-Scholes ($\sigma = 0.20$) (no bubble). Bottom-left: CEV ($\beta = 1.5, \sigma = 0.16$). Bottom-right: SABR ($\beta = 1,\ \rho = 0.7, \sigma_0 = 0.25$). The far-OTM plateau of the observed curve estimates the bubble gap $m(T)$.

From Figure 3.2 we can confirm the bubble gap mechanism using the option surface from options sheets generated by the three models respectively as defined in subsection (3.2.2). Fitting an arbitrage-free decreasing-convex call curve to the Monte-Carlo prices, we can see that the far out-the-money (OTM) segment (large K) converges to $m(T)$ as $K \to \infty$ for all models, expected from the literature. Averaging the largest $m = \lceil 0.2\,n \rceil$ fitted values, our tail fraction $\widehat{L}_{\text{tail}}$ yields a tail-plateau estimator $\widehat{m}_{\text{tail}}$ that matches $\widehat{m}_{\text{mean}}$ to within sampling error for the Black-Scholes model ($\widehat{m}^{BS}_{\text{tail}}(T) = 0$) with the SABR model lying closely outside this boundary ($\widehat{m}^{SABR}_{\text{tail}}(T) = 7.688$). However, for the CEV model we observe a gap that is significant ($\widehat{m}^{CEV}_{\text{tail}}(T) = 50.492$) when we only have strike prices up to $K = 300$. This suggests that in order for the CEV estimate to plateau we require extreme strike prices with $K \gg 300$, which in practice is unrealistic.
To calculate if these values were well within the 95% confidence interval we calculated for $\widehat{m}_{mean}(T)$ using the bootstrap method. This is precisely the strike-independent shift predicted by $C(K,T) = C^*(K,T) + m(T)$, as the bubble lifts the tail by a constant $m(T)$ without distorting the slope or curvature as clearly represented by Figure 3.2.

To summarise, in the Black–Scholes benchmark we find $m(T) \approx 0$ and the one–sided bootstrap test does not reject H_0. In both the CEV ($\beta = 1.5$) and SABR ($\beta = 1,\ \rho = 0.7$) settings we obtain $m(T) > 0$ and reject H_0 at the 95% CI level. Across all models, the mean–shortfall $\widehat{m}_{\text{mean}}(T) = S_0 - \widehat{\mathbb{E}}_{\mathbb{Q}}[S_T]$ and the far–OTM tail estimator $\widehat{m}_{\text{tail}}(T)$ agree within or close to the sampling error except where the limitation of strike grid size prevents a full plateau (CEV), consistent with the theory in Chapter 2.

To summarise, in the Black-Scholes benchmark we find that $m(T) = 0$, and the one-sided bootstrap test does not reject $H_0 : m(T) = 0$. By contrast, both the CEV model with $\beta = 1.5$, and the SABR model with $\beta = 1$ and $\rho = 0.7$, produce strict-local-martingale behaviour with $m_{\text{mean}}(T) > 0$, and the test rejects accordingly. Therefore, with 95% confidence we conclude that $m(T) > 0$ in the CEV and SABR models with these parameters. Across all models, the two estimators of the bubble gap the mean-shortfall $\hat{m}(T) = S_0 - \widehat{\mathbb{E}}_{\mathbb{Q}}[S_T]$ and the far-OTM tail from a decreasing-convex call fit agree with the theory outlined in Chapter 2.

3.3 Testing m(T) with Delta bands

Noticeably, using the top 20% of the tail to gain $\widehat{m}_{\text{tail}}$ in real markets presents an obvious problem. In real markets extremely far OTM call options are rarely traded and as such the data for them is scarce. This could lead to our 20% including calls that are ITM pushing up the estimate for $\widehat{m}_{\text{tail}(T)}$ extortionately. Additionally, another problem we face

is that since OTM call options are usually illiquid and trade infrequently, when there is data for them, its could be an inaccurate representation of that true value of the call price. From these issues, we decide to adapt our tests to instead estimate $m(T)$ using only Delta band to specify a group of observed strikes and the slope of the observed call surface. Classified as one of the options pricing greeks, Delta represents the measure of sensitivity of an option's price to changes in the underlying asset. Formally, Delta can be defined under Black and Scholes (1973) as

$$\Delta = \frac{\partial C(K,T)}{\partial S_0}, \qquad \text{for fixed } (K,T,r,d,\sigma)$$

The property of delta that makes it of interest to us is that it is monotone in strike ($\Delta \downarrow$ as $K \uparrow$). This means that deep ATM (ITM) calls will have $\Delta \approx 1$, at the money (ATM) calls will have $\Delta \approx 0.5$ and deep OTM calls have $\Delta \approx 0$. We aim to exploit this monotonicity to select a delta band of liquid strikes. In practice, market quote sheets normally report the Black-Scholes Delta computed at the option's implied volatility $\sigma_{IV}(K,T)$ and are calculated from Black and Scholes (1973) as such,

Definition 3.3.1 (Black-Scholes pricing formula and delta)**.** *Fix maturity $T > 0$, spot $S_0 > 0$, strike $K > 0$, risk–free rate r, dividend rate d, and volatility $\sigma > 0$. The Black-Scholes call prices are then*

$$C(S_0,K,T;\sigma,r,d) = S_0\, e^{-dT}\, \Phi(d_1) \;-\; K\, e^{-rT}\, \Phi(d_2),$$
$$P(S_0,K,T;\sigma,r,d) = K\, e^{-rT}\, \Phi(-d_2) \;-\; S_0\, e^{-dT}\, \Phi(-d_1),$$

where

$$d_1 = \frac{\ln(S_0/K) + (r - d + \frac{1}{2}\sigma^2)T}{\sigma\sqrt{T}}, \qquad d_2 = d_1 - \sigma\sqrt{T},$$

and Φ denotes the standard normal CDF. Since deltas are the sensitivities with respect to spot,

$$\Delta = \frac{\partial C(S_0,K,T,\sigma,r,d)}{\partial S_0} = e^{-dT}\, \Phi(d_1). \tag{3.3.1}$$

In sections where we set $r = d = 0$ this simplifies to

$$C = S_0\, \Phi(d_1) - K\, \Phi(d_2), \qquad \Delta = \Phi(d_1),$$

with $d_1 = \dfrac{\ln(S_0/K) + \frac{1}{2}\sigma^2 T}{\sigma\sqrt{T}}$ *and* $d_2 = d_1 - \sigma\sqrt{T}$.

With real market data, it is possible that Delta's on the call sheets can sometimes be missing due to data loss. To counteract this, using the fact that most call sheets are

priced using the Black-Scholes model we will implement (3.3.1) to produce replacements for Delta when needed.

From the partial derivative identities we discussed earlier in Section 1.2 we are able to define the slope of the observed call surface. Letting $q(K) = \mathbb{Q}(S_T \geq K)$ we recall from Section 1.2, the fundamental call satisfies,

$$C^*(K,T) = \int_K^\infty q(u)\,du, \qquad -\frac{\partial C^*}{\partial K}(K,T) = q(K), \qquad \mathbb{E}_\mathbb{Q}[S_T] = \int_0^\infty q(K)\,dK.$$

Observed calls satisfy $C = C^* + m(T)$, so the derivatives are unchanged,

$$\frac{\partial C}{\partial K}(K,T) = \frac{\partial C^*}{\partial K}(K,T) = -q(K)$$

Therefore, if we are able to learn $q(K)$ from given quotes and bound it elsewhere using only no-arbitrage shape, we can integrate to get $\mathbb{E}_\mathbb{Q}[S_T]$ and then $m(T) = S_0 - \mathbb{E}_\mathbb{Q}[S_T]$. With discrete, noisy quotes we cannot differentiate naively, so on a stable window of strikes we fit an arbitrage–free call curve $\widehat{C}^*(K,T)$ that is decreasing and convex (no static arbitrage). In practice we do this by projecting finite differences onto the cone $\{q_i \geq 0,\ q_{i+1} \leq q_i\}$ using isotonic regression as before $q_i \approx (C_{i-1} - C_i)/(K_i - K_{i-1}))$ the key difference is that the fit uses only shape constraints, not a pricing model. We then define $\widehat{q}(K,T) = -\frac{\partial \widehat{C}^*}{\partial K}(K,T)$ and integrate it ($\int \widehat{q}\,dK$), giving an estimate of the contribution of that strike window to $\mathbb{E}_\mathbb{Q}[S_T]$. Outside this window we bound the unknown tail areas using only shape (monotonicity and non-negativity of q) and the observed level $C(K_N,T)$ at the right edge. We also wish to implement a Delta band selection, where we choose a band $\Delta \in [\Delta_{\min}, \Delta_{\max}]$ that only implements strikes in this range into our algorithm.

3.3.1 Delta band estimator for m(T)

First, we fix a any Delta window $[\Delta_{\min}, \Delta_{\max}] \subset (0,1)$. Using the deltas from the market or Black-Scholes calculated data, this selects an in-band strike interval $[K_0, K_N]$ around the money where quotes are liquid. On this band we:

1. Fit a decreasing, convex call curve $K \to \widehat{C}^*(K,T)$ through the in-band quotes. We define

$$\hat{q}_{\text{band}}(K) = -\frac{\partial \widehat{C}^*}{\partial K}(K,T), \qquad K \in [K_0, K_N]. \tag{3.3.2}$$

   Because $\widehat{C}^*(K,T)$ is convex and $\frac{\partial \widehat{C}^*}{\partial K}(K,T)$ is non increasing, $0 \leq \hat{q}_{\text{band}} \leq 1$.

2. Extend to the wings under no-arbitrage. We only impose that q is non-increasing

$q(0) \le 1$, $q(\infty) = 0$. At the in-band edges we know,

$$q_0 \equiv \hat{q}_{\text{band}}(K_0), \qquad q_N \equiv \hat{q}_{band}(K_N).$$

On the left wing $[0, K_0)$ the set of admissible q's is

$$\mathcal{Q}_L = \{\, q : [0, K_0] \to [0, 1] : q \text{ non-increasing}, \, q(K_0) = q_0\}.$$

On the right wing (K_N, ∞) similary

$$\mathcal{Q}_R = \{\, q : [K_N, \infty) \to [0, 1] : q \text{ non-increasing}, \, q(K_N) = q_N, \, q(\infty) = 0\}.$$

3. Integrate the combined curve. For any $q_L \in \mathcal{Q}_L$ and $q_R \in \mathcal{Q}_R$,

$$\widehat{\mathbb{E}}[S_T](q_L, q_R) \;=\; \underbrace{\int_0^{K_0} q_L(K)\, dK}_{\text{left}} \;+\; \underbrace{\int_{K_0}^{K_N} \widehat{q}_{\text{band}}(K)\, dK}_{A_{\text{band}}} \;+\; \underbrace{\int_{K_N}^{\infty} q_R(K)\, dK}_{\text{right}},$$

with $\hat{m}(T) = S_0 - \hat{\mathbb{E}}[S_T](q_L, q_R)$. Producing an identification region for $m(T)$ across all admissible wings.

To turn the stitched mean into identification bounds we minimise and maximise $\widehat{\mathbb{E}}[S_T](q_L, q_R)$ over all $q_L \in \mathcal{Q}_L$ and $q_R \in \mathcal{Q}_R$. Because the objective is linear and the admissible sets are convex under the monotonicity constraints, the extrema are attained at the boundaries, where the left wing at $q \equiv q_0$ (min) and $q \equiv 1$ (max), on the right wing at the smallest tail $q \equiv 0$ (min) and at the largest tail consistent with the observed level $C_{\text{obs}}(K_N, T)$ (max). The following proposition records the resulting closed-form bounds.

Proposition 3.3.2. *(Closed form identification bounds from shape) Let*

$$A_{band} = \int_{K_0}^{K_N} \widehat{q}_{band}(K)\, dK, \qquad C_{obs}(K_N, T) \text{ be the observed call at } K_N.$$

Then

$$\underline{\mathbb{E}} = \inf_{q_L \in \mathcal{Q}_L,\, q_R \in \mathcal{Q}_R} \widehat{\mathbb{E}}[S_T] \;=\; \underbrace{q_0 K_0}_{\min \textit{left}} + A_{band} + \underbrace{0}_{\min \textit{right}},$$

$$\overline{\mathbb{E}} = \sup_{q_L \in \mathcal{Q}_L,\, q_R \in \mathcal{Q}_R} \widehat{\mathbb{E}}[S_T] \;=\; \underbrace{K_0}_{\max \textit{left}} + A_{band} + \underbrace{\int_{K_N}^{\infty} q \;\le\; C_{obs}(K_N, T)}_{\max \textit{right}}.$$

Consequently, the identification interval for the bubble gap is,

$$[m_{\max},\, m_{\min}] = [\, S_0 - \overline{\mathbb{E}}, \;\; S_0 - \underline{\mathbb{E}}\,] =$$

$$\Big[\, S_0 - (K_0 + A_{band} + C_{obs}(K_N, T)), \;\; S_0 - (q_0 K_0 + A_{band})\,\Big].$$

Proof. We prove this interval from the left and right wings as follows,

Left wing: q is non-increasing on $[0, K_0]$ with $q(K_0) = q_0 \in [0, 1]$. Hence $q(K) \geq q_0$ for all $K < K_0$, so $\int_0^{K_0} q\, dK \geq q_0 K_0$ with equality for the flat curve $q \equiv q_0$. For the maximum, take $q(K) = 1$ for $0 \leq K < K_0$ and $q(K_0) = q_0$ (a downward jump at K_0 is allowed); singletons do not affect the integral, so $\int_0^{K_0} q\, dK = K_0$.

Right wing: Non-increasing to 0 allows an immediate drop to zero: set $q(K_N) = q_N$ and $q(K) = 0$ for $K > K_N$, which yields the minimal tail area 0. For the upper bound, recall

$$C^*(K_N, T) = \int_{K_N}^{\infty} q(K)\, dK \leq C_{\text{obs}}(K_N, T),$$

because observed calls satisfy $C_{\text{obs}} = C^* + m(T)$ with $m(T) \geq 0$. Combining the left and right bounds gives

$$\underline{\mathbb{E}} = q_0 K_0 + A_{\text{band}}$$

and $\overline{\mathbb{E}} = K_0 + A_{\text{band}} + C_{\text{obs}}(K_N, T)$, and hence the stated identification interval for $m(T) = S_0 - \mathbb{E}_Q[S_T]$. □

From these bounds we can see that the width of $[m_{\max}, m_{\min}]$ equals,

$$\text{width} \;=\; (1 - q_0)\, K_0 \;+\; C_{\text{obs}}(K_N, T),$$

which is dominated by the left term. If the band includes deep ITM strikes (so $q_0 \approx 1$ and K_0 is not large), this interval collapses. The right term can be made arbitrarily small by choosing K_N so that $C_{\text{obs}}(K_N, T)$ is tiny. This shows that using only ATM and deep ITM quotes suffice for estimation as they pin down the left area and the right tail is negligible. For any K_N in the band,

$$\int_{K_N}^{\infty} q(K)\, dK = C^*(K_N, T) \leq C_{\text{obs}}(K_N, T). \tag{3.3.3}$$

Thus the entire right wing contribution is bounded by the single observed call at the band's right edge. For example, in practice choosing K_N so that $C_{\text{obs}}(K_N) \lesssim \$0.10$ would make the right tail error negligible with no far OTM quotes needed.
If rates/dividends are nonzero ($r \neq 0, d \neq 0$), we use the following identities,

$$C^*(K, T) = e^{-rT}\, \mathbb{E}_Q[(S_T - K)^+], \qquad \partial_K C^*(K, T) = -e^{-rT}\, Q(S_T \geq K), \qquad e^{rT} C^*(0, T) = \mathbb{E}_Q[S_T].$$

All formulas above hold with the $e^{\pm rT}$ factors. When this is the case, the identification interval becomes,

$$[m_{\max}, m_{\min}] = \Big[\, S_0 - e^{-rT}(K_0 + A_{\text{band}} + C_{\text{obs}}(K_N)),\;\; S_0 - e^{-rT}(q_0 K_0 + A_{\text{band}}) \,\Big],$$

with $q_0 = -\partial_K C^*(K_0, T)\, e^{rT}$ the tail level at K_0. When we implement this model on market data in Section 3.4.2 we work with $r \neq 0, d = 0$. Before we implement our model, we first design tests to ensure that our code is robust and reliable. The first of these tests is a No-arbitrage check that ensures that $C^{\text{fit}}_{\text{obs}}$ is decreasing and convex. We do this by ensuring that $\frac{\partial C^*}{\partial K}(K,T) \leq 0$ and $\frac{\partial^2 C^*}{\partial K^2}(K,T) \geq 0$. Secondly, we check that $-\frac{\partial C^*}{\partial K}(K,T) = q(K) \in [0,1]$, and if this holds, we check the identity $\mathbb{E}[S_T] = \int_0^\infty q(K)\, dK$ by simple numerical integration, ensuring that our mean implied from the slope of the call curve matches the estimators $\widehat{\mathbb{E}}[S_T](q_L, q_R)$. We find that in our code all of these hold true, and as such, we can confidently say that these features of the model have been implemented correctly.

3.4 Implementation of the Delta band estimator

3.4.1 Testing the Delta band estimator in the CEV model

Applying this framework to the CEV model with the same parameters as in Section 3.2, we wish to see if we can recover a more accurate $\widehat{m}_{\text{tail}}$. From 3.3, using the full Delta band ($\Delta \in [0,1]$), we recover $\hat{m}(T) = 44.20$ and immediately observe that this falls comfortably within the 95% Confidence interval bounds as within 3.1 as compared to our previous tests. This is due to the change in our tail estimator rather than just the Delta method alone. Having changed the tail estimate to extrapolate from our points rather than take the average of the largest 20% of strikes, we can see that our curve extrapolates further past the last quote converging to a more accurate $m(T)$ with the same amount of quotes. To achieve this on the method implemented in Section 3.2, strikes unnaturally OTM and not possible in real markets would be needed before any average of the top 20$ of strikes could be considered a feasible estimate for $\hat{m}(T)$. Furthermore, because we were taking an average of the top 20% of quotes, the quotes at either end of this band could wildly differ pushing our estimate further from the true value of $\widehat{m}_{tail}$. Having now implemented a more robust estimate on the whole data set, we can now confidently investigate the effects that our delta band will have.

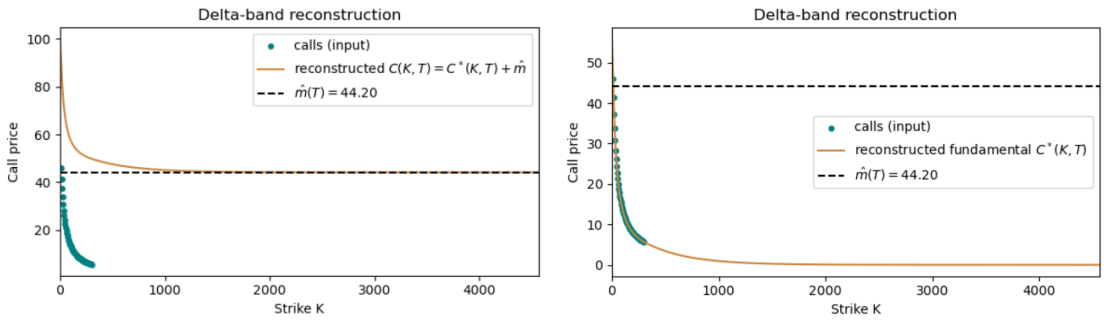

Figure 3.3: CEV call quotes (teal) projected onto the fundamental call curve $C^*(K,T)$ (orange) calculated using the delta band $[0,1]$. The dashed line shoes the estimated martingale defect $\hat{m}(T) = 44.20$. Left : reconstructed observed curve $C(K,T) = C^*(K,T) + \hat{m}(T)$, aligning with market prices in discounted units. Right : the fundamental curve $C^*(K,T)$ alone, the market curve that has been vertically shifted by the factor $\hat{m}(T)$

Since we know that having all quotes in a real market is highly unlikely, we begin by investigating ATM quotes as these are the most liquid and accurate in practice. Testing a realistic ATM band, we choose $\Delta \in [0.40, 0.60]$ and, from Figure 3.4, we obtain the estimate $\widehat{m}(T) = 32.03$. We can see that this estimate varies considerably on this range of quotes, compared to the full call surface.

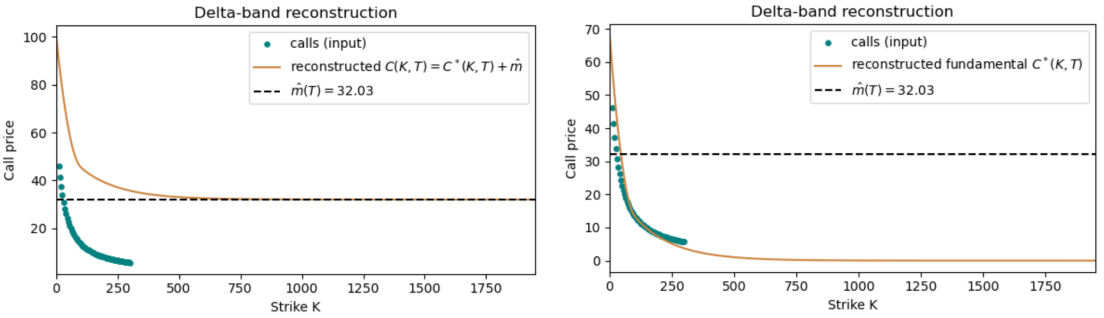

Figure 3.4: CEV call quotes (teal) projected onto the fundamental call curve $C^*(K,T)$ (orange) calculated using the delta band $[0.40, 0.60]$. The dashed line shoes the estimated martingale defect $\hat{m}(T) = 44.20$. Left : reconstructed observed curve $C(K,T) = C^*(K,T) + \hat{m}(T)$, aligning with market prices in discounted units. Right : the fundamental curve $C^*(K,T)$ alone, the market curve that has been vertically shifted by the factor $\hat{m}(T)$

The discrepancy in our estimate can be largely explained by the theory that was discussed earlier, where we found that using only ATM and deep ITM quotes suffices as an accurate estimate for our tail. We can see this in practice in Figure 3.5 where using only the band $\Delta \in [0.50, 1.00]$ we achieve the same estimate as when we using the whole call surface. In practice, this means that as long as we can find reliable ATM quotes and a selection of deep ITM quotes, we can confidently and accurately reconstruct $C^*(K,T)$.

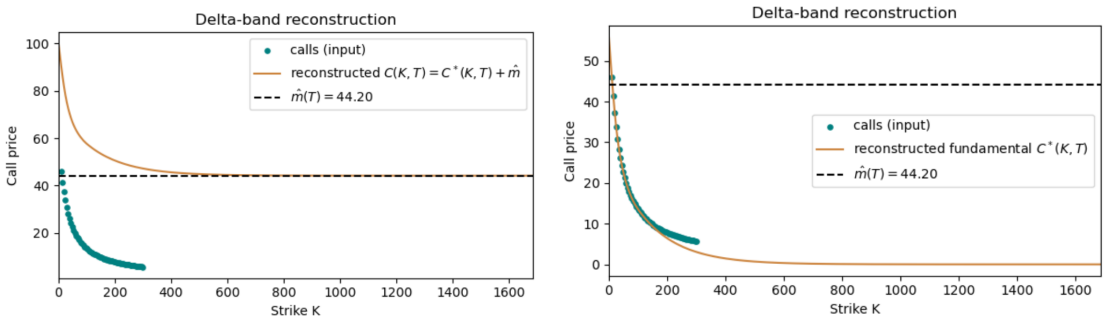

Figure 3.5: CEV call quotes (teal) projected onto the fundamental call curve $C^*(K,T)$ (orange) calculated using the delta band $[0.4, 0.6]$. The dashed line shoes the estimated martingale defect $\hat{m}(T) = 44.20$. Left: reconstructed observed curve $C(K,T) = C^*(K,T) + \hat{m}(T)$, aligning with market prices in discounted units. Right: the fundamental curve $C^*(K,T)$ alone, the market curve that has been vertically shifted by the factor $\hat{m}(T)$.

Having verified the tools used to implement this method, we now move to real market data, investigating the call sheets of Nvidia to deduce whether there exists a martingale defect.

3.4.2 Implementing the Delta band estimator on Nvidia

All of the data used within this section has been obtained from the Chicago Board Options Exchange (CBOE) Cboe (2025). Accordingly, these option sheets that we study provide a reasonable proxy for prevailing market conditions at the time they were taken. The options sheets utilised within this section can be found in Appendix D. Furthermore, to enhance an actual representation of market conditions, we introduce a risk free rate that is non negative. We obtain this rate from Trading Economics (2025). From this, we see that on the day these options were taken from the market the interest rate was 4.5%. We now set our constant risk free rate $r = 0.045$ and use this in our calculations while also ensuring that our models now contain $e^{\pm rT}$ where appropriate.

Before we are able to use our estimator for $m(T)$ on Nvidia, we must first clean our call sheet for any discrepancies (e.g. Missing Delta values). Parsing the CBOE sheet, we first extract the difference in days between the quote date and expiry of the option sheet, and divide this over 365 days to obtain a value for T. We do this as to obtain T on a scale that the maturity is measured in years. Prices are then taken as the mid-price of the call bids and asks, removing any that are not available from our data set. Where Delta's are missing from our data, we use the formula presented in Definition 3.3.1 to recover an accurate value that would appear there naturally under the Black-Scholes pricing formula.

We define the price of a call as the midpoint between the bid and ask price as when we take option prices from the market there are instances where the last traded option prices do not decrease as K increases. This is due to some of the options having last traded at a

much earlier date where the price was completely different price of what they would fairly trade for today. This method therefore ensures that pricing presents the current price of each option across all strikes K.

Implementing our method to estimate $\hat{m}(T)$ on Nvidia options, we first start with the band $\Delta = [0.50, 0.70]$ where Delta is reasonably ATM on an options sheet with the expiration date as 19th of September 2026. From figure 3.6 we can clearly see that using ATM Delta presents signs that a potential martingale defect may exists, with $\hat{m}(T) = 16.69$. With the spot price of $S_0 \approx 169.84$, this implies $\hat{\mathbb{E}}[S_T] = S_0 - \hat{m} \approx 153.15$, a reduction of around 9.8% relative to the spot. Overall, this fit suggests that there may be a positive martingale defect present at this maturity, subject to our assumptions and data cleaning techniques.

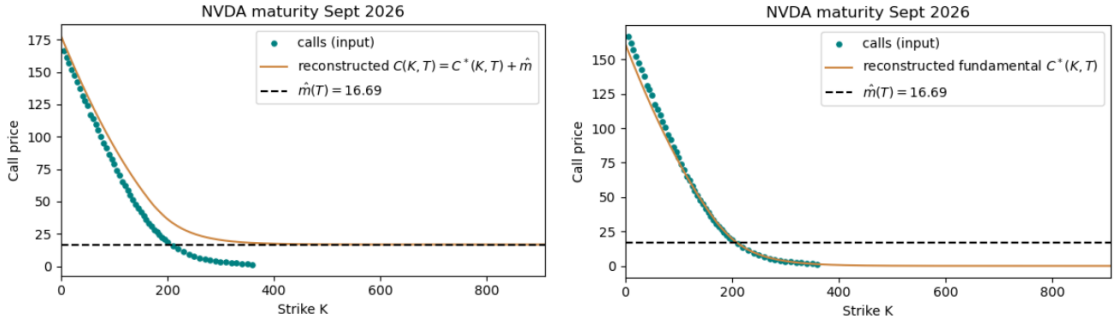

Figure 3.6: Delta-band estimator ($\Delta = [0.50, 0.70]$) for Nvidia options with expiry 19 Sep 2026. Market call quotes (teal), fundamental curve $C^*(K,T)$ (orange), martingale defect $\hat{m}(T) = 16.69$ (dashed line). Left: reconstructed observed curve $C(K,T) = C^*(K,T) + \hat{m}$. Right: the fundamental curve $C^*(K,T)$ alone.

Taking this test a step further, we test the robustness of this martingale defect across a range of maturities and Delta bounds. The Delta bounds that we select are split into three ranges of maturities, these consist of an ATM bound $\Delta_{ATM} = [0.40, 0.55]$, a slightly ITM bound $\Delta_{ITM} = [0.50, 0.70]$ and an bound consisting of ATM and far ITM quotes $\Delta_{FITM} = [0.50, 0.90]$. As we go further ITM we increase the bound of the Delta to ensure that ATM quotes are incorporate into this as well. We test on call sheets with expiries of September 2026, December 2026, January 2027, June 2027, December 2027. These maturities were chosen as due to the limited access of options data as a student we are unable to obtain all maturities, so utilise the ones we can.

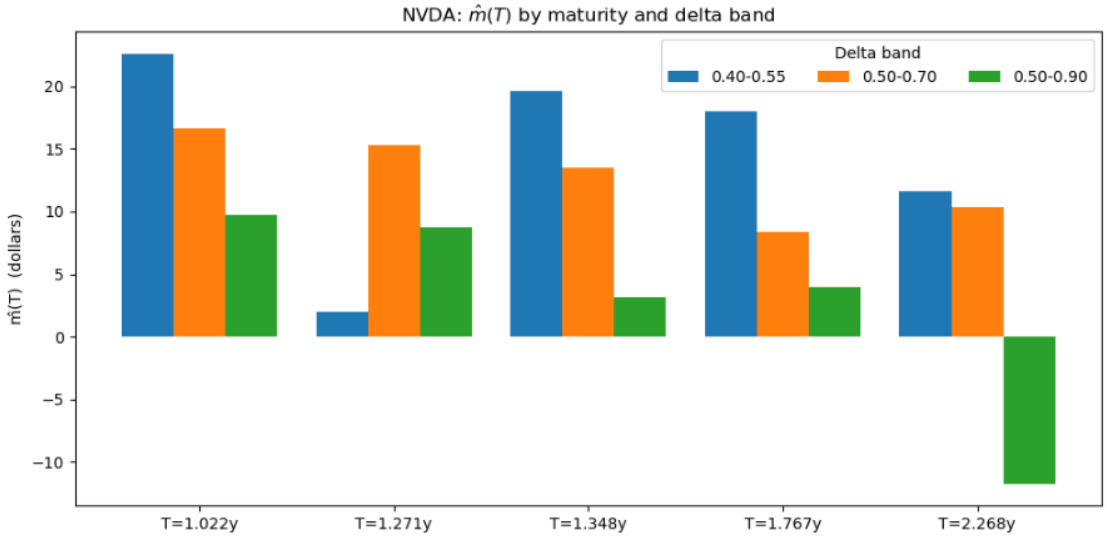

Figure 3.7: NVDA: $\hat{m}(T)$ by maturity and spot-delta band. Each group shows estimates for Δ_{ATM}, Δ_{ITM}, and Δ_{FITM} at the indicated maturity.

Figure 3.7 demonstrates the results we achieve for these runs and observably for the range of all Delta bounds up to the maturity for June 2027, the martingale defect estimate $\hat{m}(T)$ is positive. The bands Δ_{ATM}, and Δ_{ITM} mostly deliver larger defects across all maturities, in comparisons to Δ_{FITM} whose effect tends to shrink overtime even yielding a negative estimate for December 2027 maturity. We also notice from Figure 3.8 that as the time to maturity increases we see that the range in between these bands increases along with it, with the median staying positive throughout all maturities. A plausible explanation for this widening of bands is due to the time value options. As the time to maturity increases there is higher probability that events, such as changes in interest rate, share issuances, and crashes will occur that will effect the price. This means that market makers will charge more for the time benefit, so spreads widen and mid price become somewhat less reliable especially for far ITM options. This is the reason why we see this band dispersion increase as time increases, and even see negative $\widehat{m}(T)$ for the widest band Δ_{FITM}.

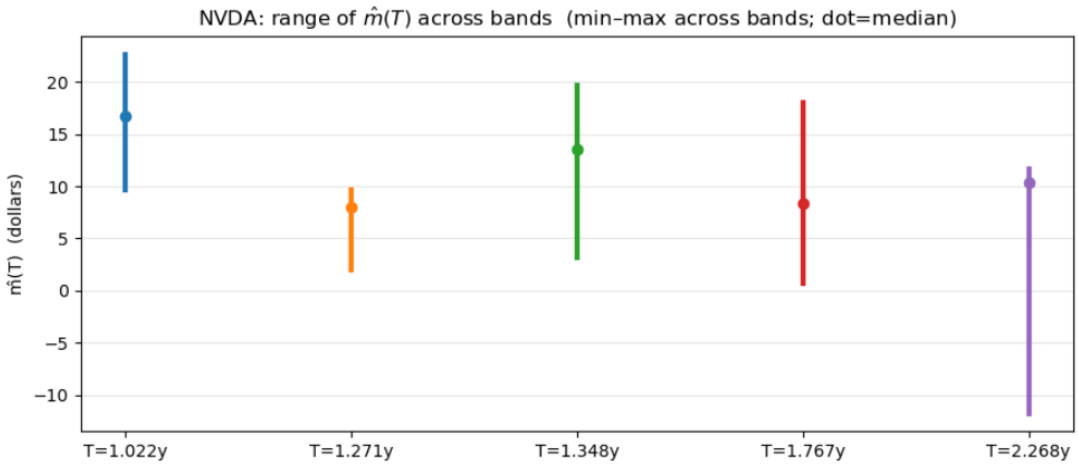

Figure 3.8: NVDA: dispersion of $\hat{m}(T)$ across spot-delta bands at each maturity. Whiskers show the minimum and maximum across $\{\Delta_{\text{ATM}}, \Delta_{\text{ITM}}, \Delta_{\text{FITM}}\}$; dots show the median.

Therefore, using the bounds Δ_{ITM} gives a more accurate estimate for $\widehat{m}(T)$ further in the future but it is still not conclusive. This is because $\hat{m}(T)$ incorporates both ITM and ATM options of which, are much more reliably priced than those far ITM. Since all bands produce a positive bubble gap $\hat{m}(T)$ at short to intermediate maturities there is evidence to support that a positive martingale effect is present, however conclusions for long dated maturities cannot be confidently made, as the results are tentative.

Throughout this chapter we have assumed that market prices are Continuous however this is not the case due to many factors such as open and close of market and spacing between a specified amount This motivates the next chapter, where we introduce jump-driven strict local martingales, in which discontinuities and state-dependent jump intensities can generate a persistent positive martingale defect.
Throughout this chapter we have idealised market prices as evolving on continuous paths. In reality, prices move in discrete jumps due to many factors including across overnight gaps and tick size discreteness. This motivates our next chapter, where we introduce jump-driven strict local martingales, models with explicit discontinuities and state dependent jump intensities that offer a structural mechanism for a persistent positive martingale defect $m(T) = S_0 - \mathbb{E}[S_T]$.

Chapter 4

Jump-Driven strict local martingales

In practice, real equities trade in discrete intervals widely known as "ticks" where Quotes in the market often move by a specified increment e.g. (0.01\$). When a sudden move such as a bubble burst occurs a massive tick change not covered by a continuous diffusion framework can occur, displaying a discontinuity in pricing. Many bubbles display price dynamics that have super-exponential run-ups with periodic corrections, a pattern consistent with positive feedback and herding rather than simple diffusion Sornette and Cauwels (2014). As such phases mature, the probability of a crash rises, implying material gap risk and tail dependence that purely continuous models struggle to capture Sornette and Cauwels (2014). Observations like these are what motivate us to move to a discontinuous model by introducing jumps into the pricing framework. Working within the no-arbitrage semi martingale setup, allowing jumps provides a direct way to represent discontinuities, fat tails and state dependent bursts, without resorting to the need for increasingly complex volatility layers that continuous models would need to make up this shortfall Sornette and Cauwels (2014).

Economically, jumps are warranted because discrete information arrivals, such as earnings surprises and policy shifts, produce discontinuous moves in prices Merton (1976). Strict local martingales with jumps however, require additional structure. For example, the arise when feedback effects make jump intensities depend on the current state (self-exciting), yielding a local but non-martingale price under the risk-neutral measure Keller-Ressel (2015), or when prices are formed on a coarser information set than the underlying process (filtration shrinkage), which induces jumps and strictness without defining a jump law Protter (2015). In these settings, with $r = d = 0$ the discounted price is a strict local martingale, producing a positive bubble gap $m(T) = S_0 - \mathbb{E}_{\mathbb{Q}}[S_T]$.

In this chapter we explore the notion of what jump process are, how they appear as strict local martingales, investigating how we could possible simulate such a process using different numerical methods and implement this.

4.1 Jump processes

Jump processes form a vital class of stochastic processes characterised by their capability to model sudden and discontinuous changes over time. Contrary to continuous processes such as Brownian motion, jump processes exhibit trajectories with discrete jumps occurring at random times, capturing phenomena with abrupt shifts in value. We formally define a jump process as follows,

Definition 4.1.1. *(Jump Process). Let $(\Omega, \mathcal{F}, (\mathcal{F}_t)_{t\geq 0}, \mathbb{P})$ be a filtered probability space satisfying the usual conditions as in chapter 1. A stochastic process $J = (J_t)_{t\geq 0}$ with càdlàg paths is called a jump process if there exsists a sequence of stopping times $(\tau_n)_{n\geq 1}$, almost surely strictly increasing to infinity, such that*

1. *The sample paths of J are constant on each interval $[\tau_n, \tau_{n+1})$ almost surely*
2. *The process J changes value only by jumps at the times τ_n i.e. for all t,*

$$J_t = J_0 + \sum_{n:\tau_n \leq t} \Delta J_{\tau_n}, \qquad \text{where } \Delta J_{\tau_n} = J_{\tau_n} - J_{\tau_n^-} \neq 0 \tag{4.1.1}$$

Thus J is piecewise constant with jump discontinuities only at the time τ_n Rogers and Williams (2000).

A fundamental example of a jump process is the Poisson process which models the random occurrence of independent events over time with exponentially distributed waiting times between jumps. We define as such,

Definition 4.1.2. *(Poisson Process). A counting process $N = \{N_t : t \geq 0\}$ is a Poisson process with rate $\lambda > 0$ if and only if,*

1. *$N_0 = 0$ almost surely*
2. *N_t has independent increments: for any $0 \leq s < t$, the number of jumps $N_t - N_s$ is independent of the past $\mathcal{F}_s$*
3. *$N_t - N_s$ follows a Poisson distribution with mean $\lambda(t-s)$, i.e.*

$$\mathbb{P}(N_t - N_s = k) = \frac{(\lambda(t-s))^k}{k!} e^{-\lambda(t-s)} \tag{4.1.2}$$

4. *Paths are right-continuous and piecewise constant, jumping by one at each event.*

Passion processes serve as the baseline model for random,memoryless event arrivals in diverse fields such as queueing, insurance claims, and high-frequency finance. To account for jumps with variable size we can extend the Poisson process by associating each jump with a random magnitude. This process is commonly known as the Compound Poisson process as presented below,

Definition 4.1.3. *(Compound Poisson Process) Let N_t be a Poisson process with intensity λ, and $\{Y_i\}$ be an independent sequence of independent and identically distributed random variables representing jump sizes. The compound Poisson process X_t is the defined as*

$$X_t = \sum_{i=1}^{N_t} Y_i \tag{4.1.3}$$

This process jumps at the arrival times of N, with jump sizes distributed according to the law of Y. Compound Poisson processes are commonly used for modelling aggregate claims in insurance, operational risk and most importantly in our case, jumps in asset prices.

Building on the concept of jump processes, Lévy processes offer a unified and far-reaching framework in stochastic process theory that encompasses both continuous and jump dynamics. A Lévy process is defined as a stochastic process with stationary and independent increments and càdlàg paths, thereby generalizing classical continuous-time models such as Brownian motion and classic jump-driven models like the Poisson process. This generality equips Lévy processes with the flexibility to capture real-world phenomena exhibiting a mixture of smooth fluctuations and abrupt discontinuities, essential for trying to capture bubbles where they commonly have discontinous points.

Definition 4.1.4. *(Lévy Process) A Lévy process is a stochastic process $X = \{X_t : t \geq 0\}$ that satisfies the following properties:*

1. $X_0 = 0$ *almost surely;*
2. *Independence of increments: For any $0 \leq t_1 \leq t_2 < \cdots < t_n < \infty$, $X_{t_2} - X_{t_1}, X_{t_3} - X_{t_2}, \cdots, X_{t_n} - X_{t_{n-1}}$ are mutually independent;*
3. *Stationary increments: For any $s < t$, $X_t - X_s$ is equal in distribution to X_{t-s};*
4. *Continuity in probability: For any $\varepsilon > 0$ and $t \geq 0$ it holds that $\lim_{h \to 0} P(|X_{t+h} - X_t| > \varepsilon) = 0$*

It is important to emphasize that while every jump process with stationary, independent increments is a Lévy process, not every Lévy process is a jump process. Specifically, the class of Lévy processes encompasses both pure-jump processes (with paths consisting entirely of discontinuities) and processes with continuous paths (such as Brownian motion), as well as processes combining both jump and continuous components. The primary focus here lies on pure-jump Lévy processes, which provide a natural and flexible foundation for modelling systems driven by random shocks or arrivals. The Lévy–Itô decomposition guarantees that any Lévy process can be uniquely represented as the sum of a Brownian motion part, a compound Poisson jump component and a purely discontinuous martingale with infinite activity of small jumps. We now illustrate this general concept of a Lévy process with a canonical example,

Example 1. The Gamma process $(\Gamma_t)_{t\geq 0}$ is a pure-jump Lévy process with stationary and independent increments. For parameters $a > 0$ (rate) and $b > 0$ (scale), the increments of the gamma process over an interval $[s, t]$ satisfy

$$\Gamma_t - \Gamma_s \sim \text{Gamma}(a(t-s), b), \qquad 0 \leq s < t, \tag{4.1.4}$$

where the Gamma distribution has density

$$f(x) = \frac{x^{a(t-s)-1}e^{-x/b}}{\Gamma(a(t-s))b^{a(t-s)}}, \qquad x > 0 \tag{4.1.5}$$

The sample paths are non-decreasing and right-continuous, with positive jumps occurring at random times.

The gamma process is a non decreasing Lévy process with Lévy measure $\nu(dx) = ax^{-1}e^{-x/b}dx$ supported on $(0, \infty)$. As such, it has infinite activity on every interval, as there are infinitely many small jumps, and no Brownian motion or drift component. Its independent and stationary increments exemplify the Lévy process definition, and the explicit form of the increments makes simulation straightforward, as demonstrated in Figure 4.1.

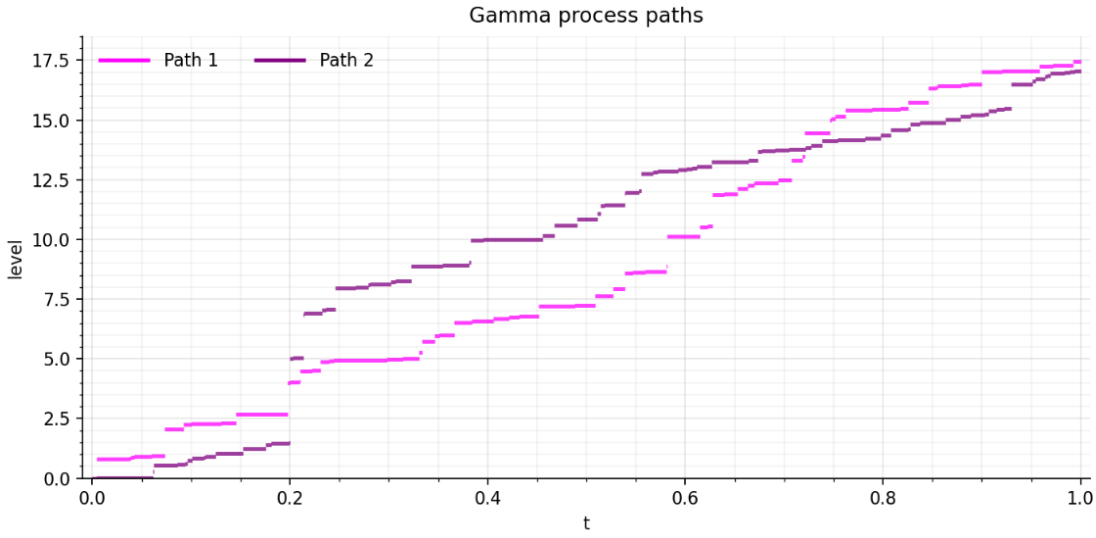

Figure 4.1: 2 paths of the gamma process

This process has various applications, being frequently used as a building block in finance for more complex asset models such as variance gamma and CGMY processes Applebaum (2009). Having established the fundamental framework of jump processes as pure-jump Lévy processes, we now turn to examining the interesting subclass of strict local martingales that arise within these jump processes.

4.2 Methods for generating jump processes with strict local martingales

Most classical examples of strict local martingales arise in the setting of continuous path processes. However, explicit constructions of jump and pure-jump strict local martingales are comparatively rare in the literature, with notable exceptions emerging only recently. In this section, we present two methods for generating strict local martingales within jump process framework. We then focus on one of these methods and implement numerical techniques to demonstrate it characteristic behaviour as a strict local martingale.

The first method, developed by Keller-Ressel (2015), introduces a class of pure-jump strict local martingales constructed as exponential of self exciting affine jump processes, where the intensity of the jump is proportional to the currently process value. This "self exciting" structure is not only mathematically natural but also financially motivated, as it reflects the feedback mechanisms believed to underlie real world asset price bubbles. Keller-Ressel (2015)'s approach achieves strict local martingale behaviour by exponentially tilting processes that would otherwise explode in finite time, by balancing the jump intensity and drift to ensure non-explosive dynamics while forfeiting the true martingale property. The second method, come from Protter (2015) where they implement the use of filtration shrinkage producing strict local martingales with jumps via restriction of observable information. We provide a brief overview of this method for insight on the other methods that can be used to produce strict local martingales with jumps, but do not rigorously define it as our foucs lies on the Keller-Ressel (2015) methodology.

This method details the explicit construction and mathematical properties of the pure-jump strict local martingale process introduced by Keller-Ressel (2015). As a highly transparent example of a self-exciting pure jump Markov process, this model illustrates how strict local martingale behaviour can arise from the combined effects of state-dependent jump intensities and a balancing negative drift. By capturing the mechanism where the likelihood of jumps increases proportionally with the process level, this class of models offers fundamental insight into the formation of bubbles and other non-linear phenomena in jump-driven systems. We first define what a Markov process is,

Definition 4.2.1. *(Markov Process) Let $X = (X_t)_{t\geq 0}$ be a stochastic process defined on a filtered probability space $(\Omega, \mathcal{F}, \{\mathcal{F}_t\}_{t\geq 0}, \mathbb{P})$ that takes values in a measure state space (E, ε).*

The process X is said to be a Markov process with respect to the filtration $(\mathcal{F}_\sqcup)_{t\geq 0}$ if for every $t \geq 0$, every measurable set $A \in \varepsilon$, and every $s \leq t$ the following holds almost surely,

$$\mathbb{P}(X_t \in A \,|\, \mathcal{F}_s) = \mathbb{P}(X_t \in A \,|\, X_s). \tag{4.2.1}$$

This expresses that the conditional distribution of the future state X_t, given the entire history up to time s depends only on the current state X_s at time s.

The core of this model lies within the choice of Lévy measure, which specifies the frequency and size of the jumps in the process. This is specified as,

$$\mu(d\xi) = \frac{1}{2\sqrt{\pi}} e^{-\xi} \xi^{-3/2} d\xi, \qquad \xi \in \mathbb{R}_{\geq 0}. \tag{4.2.2}$$

Here, $\mu(d\xi)$ decays for large jumps but is singular at zero, which guarantees both frequent small jumps and rare large jumps, a trait common with infinite activity pure-jump processes. Now, we consider the Feller process on the state space $\mathbb{R}_{\geq 0}$ defined by the generator

$$\mathcal{A}f(x) = -\frac{x}{2} f'(x) + x \int_0^\infty (f(x+\xi) - f(x) - f'(x)\xi)\mu(d\xi), \tag{4.2.3}$$

Where this formula holds for all function f belonging to the core $C_c^\infty(\mathbb{R}_{\geq 0})$.
According to Theorem 2.7 in Duffie, Filipović and Schachermayer (2003), there exists a Feller process that can be realized as a càdlàg, adapted strong Markov process X defined on a filtered probability space $(\Omega, \mathcal{F}, \{\mathcal{F}_t\}_{t\geq 0}, \mathbb{P})$ that satisfies the usual conditions. The model is conservative, non-negative and affine by construction and throughout we assume a non-zero deterministic initial value $X_0 > 0$ to avoid trivial cases. This generator can be split up into two terms that we are both interested in, the first term $-\frac{x}{2} f'(x)$ represents a linear negative drift, pulling the process towards zero at a rate proportional to its current value. The second longer term describes the state dependent (self-exciting) jumps, the higher the state is at x, the greater the rate of all jump sizes, distributed according to μ. Furthermore, from Duffie, Filipović and Schachermayer (2003) we can see that this process X is known to be a semi martingale with explicitly computable characteristics. Relative to the truncation function $h(x) = x$ these are defined as,

$$B_t(\omega) = -\frac{1}{2} \int_0^t X_s(\omega) ds, \tag{4.2.4}$$

$$C_t(\omega) = 0, \tag{4.2.5}$$

$$\nu(\omega, d\xi, ds) = X_{s-}(\omega)\mu(d\xi)ds. \tag{4.2.6}$$

Where B_t represents the drift/finite variation part, C_t is the continuous martingale covariance which is zero for this model, and ν is the predictable compensator for the process jumps as the rate of jumps of size $d\xi$ at time s is $X_{s-}\mu(d\xi)$. Letting $J(\omega, d\xi, ds)$ denote the random measure of jumps and $\overline{J}(\omega, X_{s-}, d\xi, ds) = J(\omega, d\xi, ds) - X_s - \mu(d\xi)ds$ for its compensated version, we can now write X as,

$$X_t = X_0 + \int_{\mathbb{R}_{\geq 0} \times [0,t]} \xi \overline{J}(\omega, X_{s-}, d\xi, ds) - \frac{1}{2} \int_0^t X_{s-} ds. \tag{4.2.7}$$

Since the law of an affine process is uniquely determined by its semi-martingale characteristics (see Duffie, Filipović and Schachermayer (2003)), we may regard X as the weak solution, unique in distribution, of this integral equation. The first term of this equation collects all upward jumps, arriving at a rate proportional to the current value X_{s-}. The second term represents the mean-reverting negative drift, counteracting the process's tendency to explode. Interpreting this behaviour we observe that the jump intensity is self-exciting. X jumps upward at a rate proportional to itself (X_{s-}), so as the process increases jumping becomes even more frequency. This is what links this process to the nature of self-reinforcing financial bubbles when they are formed by herding and FOMO. To ensure that the process does not explode to infinity the upward movement is offsent by both the jump compensator and the deterministic drift.

A key property that is contained within this process is that of infinite activity but finite variation. This is due to the fact that,

$$\int_0^\infty \mu(d\xi) = \frac{1}{2\sqrt{\pi}} \int_0^\infty e^{-\xi} \xi^{-3/2} d\xi = \infty, \tag{4.2.8}$$

so this process has infinitely many samll jumps in finite time. However since,

$$\int_0^\infty \xi\mu(d\xi) = \frac{1}{2\sqrt{\pi}} \int_0^\infty e^{-\xi} \xi^{-1/2} d\xi = \frac{1}{2}, \tag{4.2.9}$$

which is finite, the total expected jump amplitude over any interval is bounded. By proposition 2.29 in Jacod and Shiryaev (1987), X is a special semi-martingale. This is interesting as with this now for X it can be shown that the process $S = e^X - 1$ is a strict local martingale, thus showing a jump-process hold a strict local martingale, important in our context within finance bubbles.

In addition to the explicit constructions based on self-exciting jump processes, another important approach to generating strict local martingales with jumps is through filtration shrinkage, as developed by Protter (2015). In this, Protter (2015) takes a strict local martingale with continuous paths on a filtered probability space $(\Omega, \mathcal{F}, \{\mathcal{F}_t\}_{t\geq 0}, \mathbb{P})$ and shows that when this is project this onto a significantly smaller filtration, also known as a subfiltration, a new process emerges. If the original filtration is sufficiently "poor" then multiple stopping times will be lost and in the new sub filtration will contain stopping times which are inaccessible. Protter (2015) classifies these inaccessible stopping times as potential jump times of a strict local martingale and illustrates that these processes can arise naturally unlike Keller-Ressel (2015)'s method.

This method is conceptually important, as Protter (2015) shows that in practice deriving from continuos strict local martingales with restricted information can produce a strict local martingale jump process. This technique reveals a fundamental concept between

filtrations and strict local martingale phenomena, emphasizing how information restriction and filtration shrinkage can induce jump discontinuities and martingale defects even when the original process is well-behaved and continuous. Conceptually, this method can interpreted in contexts such as when a market participant does not observe the full information set of an asset but instead observes a smaller filtration of this. Consequently, the observable price process is the projection of the true continuous process onto this reduced filtration. While the original process may be continuous, the projection onto the smaller filtration often displays jump discontinuities representing the sudden arrival of information previously hidden from the market participant. Therefore, the jumps in the projected process reflect information surprises practically in the market these can be represented as, but are not limited to, earning releases or sudden policy changes. These encapsulates unpredictable behaviour induced by partial market observability, producing a strict local martingale that corresponds to bubble phenomena under limited information.
Having outlined the theoretical foundation and construction methods for strict local martingales arising within jump process frameworks, we now turn to a concrete example from Keller-Ressel (2015) to demonstrate a pure-jump process with strict local martingale behaviour. This serves as a explicit illustration of the complex dynamics underlying bubble phenomena in jump-driven markets.We expand on this further by using numerical methods to demonstrate practically the concepts and characteristics of this process.

4.3 Example of a strict local martingale with pure-jumps

Following Keller-Ressel (2015), we work with $S_t = e^{X_t} - 1$ and, starting from Keller-Ressel (2015)'s lemma 2.1 and its closed form $\mathbb{E}[S_t]$ that produces a strict local martingale, we recover distributions for suitable for simulation and generate accurate paths to visualise this strict local martingale with pure jumps. Keller-Ressel (2015)'s lemma 2.1 is defined as follows

Lemma 4.3.1. *The process $S = e^x - 1$ is a local martingale and*

$$\mathbb{E}[e^{uX_t}] = exp\{X_0(1 - (w(u)e^{-t/2} - 1)^2)\} \qquad for\ all\ u < 1 \tag{4.3.1}$$

where $w(u) = 1 - \sqrt{1-u}$.

If this lemma is true then by monotone convergence

$$\mathbb{E}[S_t] = \mathbb{E}[e^{X_t}] - 1 = \lim_{u \to 1} \mathbb{E}[e^{uX_t}] - 1 = \exp(X_0 e^{-t/2}(2 - e^{-t/2})) - 1 \tag{4.3.2}$$

As a local martingale with non-constant expectation S must then be a strict local martingale, the full proof for this can be found in Keller-Ressel (2015).

Since we know that $S = e^x - 1$ is defined as a strict local martingale we can now use a inverse Laplace transform method to obtain the density in order to generate data from this model. First we derive the density f_{X_t} theoretically by Laplace inversion (Bromwich integral, evaluated numerically via the Abate-Whitt algorithm). For simulation, we use the analytically equivalent Fourier inversion implemented with the COS method coined by Fang and Oosterlee (2008), based on the conditional characteristic function $\phi_{t,x}(\omega) = \exp\{x\, g(t, i\omega)\}$. Both routes recover the same transition law however we use the COS method in our code for speed and stability.

Proposition 4.3.2. *Let X_t be a real valued random variable with density f_X. Define $S = e^{X_t} - 1$. Then S is supported on $(-1, \infty)$ and has density,*

$$f_S(s) = \begin{cases} \frac{f_X(log(1+s))}{1+s}, & s > -1 \\ 0, & s \leq -1 \end{cases} \tag{4.3.3}$$

Proof. For $\Re u < 1$

$$M_X(u) = E[e^{uX_t} \mid X_0 = x_0] = \exp\{x_0[1 - (e^{-\frac{t}{2}}(1 - \sqrt{1-u}) - 1)^2]\} \tag{4.3.4}$$

so the Laplace transform of X_t is,

$$\mathcal{L}_X(s) = \mathbb{E}[e^{-sX_t}] = M_X(-s), \qquad \Re s > 0 \tag{4.3.5}$$

We now apply an integral formula for the inverse Laplace transform known as the Bromwich integral, which gives,

$$f_X(x) = \frac{1}{2\pi i} \int_{\sigma - i\infty}^{\sigma + i\infty} e^{sx} \mathcal{L}_X(s) ds, \qquad \sigma > 0 \tag{4.3.6}$$

Numerically applying the trapezoidal rule B.1.1 according to Abate and Whitt (1992) , for any $x > 0$,

$$f_X(x) \approx \frac{e^{A/2}}{x} \left[\frac{1}{2} \Re \mathcal{L}_X\left(\frac{A}{x}\right) + \sum_{k=1}^{K} (-1)^k \Re \mathcal{L}_X\left(\frac{A + k\pi i}{x}\right) \right] \tag{4.3.7}$$

A is the shift in Bromwich contour chosen so that all $\mathcal{L}_X(s)$ lie to the left of $\Re(s) = \frac{A}{x}$. K is the number of terms in the alternating sum. Increasing K reduces the truncation error of the infinite series at the cost of evaluating $\mathcal{L}_X$ more times. In practice the usual choices for A and K are 18 and 32 respectively (Abate and Whitt, 1992). Since $g(x) = e^x - 1$ is strictly increasing on $\mathbb{R}$, it has the inverse $g^{-1}(s) = \log(1 + s)$ defined for $s > -1$. For any Borel set $A \subset (-1, \infty)$

$$\mathbb{P}(S \in A) = \mathbb{P}(X \in g^{-1}(A)) = \int_{g^{-1}(A)} f_X(x)\, dx, \tag{4.3.8}$$

substituting $x = g^{-1}(s) = \log(1+s)$ and $dx = \frac{1}{1+s}\,ds$ we get,

$$\mathbb{P}(S \in A) = \int_A f_X(\log(1+s))\frac{1}{1+s}ds. \tag{4.3.9}$$

Therefore the density when S exists on $(-1, \infty)$ is

$$f_S(s) = \frac{f_X(\log(1+s))}{1+s}, \qquad s > -1. \tag{4.3.10}$$

□

Because the Bromwich inversion is numerically heavy for path simulation, we produce an equivalent Fourier and COS derivation following Fang and Oosterlee (2008) that produces the same density but allows for more rapid and accurate sampling. Given a current state x and step $\Delta > 0$, the conditional Fourier transform ("characteristic function") of $X_{t+\Delta} \mid X_t = x$ is

$$\phi_{x,\Delta}(\omega) = \mathbb{E}\big[e^{i\omega X_{t+\Delta}} \mid X_t = x\big] = \exp\{\, x\, g(\Delta, i\omega)\,\}, \tag{4.3.11}$$

we then apply the COS reconstruction as in (B.2.0)-(B.2.2) with $\phi_Z = \phi_{x,\Delta}$. Since $X \geq 0$, we use the standard "state aware" cumulant window (i.e. the generic rule (B.2.3) adapted to the support.

$$a = 0, \qquad b = c_1 + L\sqrt{c_2}, \qquad c_1 = \kappa'(0), \quad c_2 = \kappa''(0), \quad \kappa(u) = x\, g(\Delta, u), \tag{4.3.12}$$

and COS coefficients

$$A_k = \frac{2}{b-a}\,\Re\left\{\phi_{x,\Delta}\Big(\frac{k\pi}{b-a}\Big)\, e^{-ik\pi a/(b-a)}\right\}, \qquad k = 0, \ldots, N-1. \tag{4.3.13}$$

On a finite interval $[a, b] \subset [0, \infty)$, the (conditional) density admits a Fourier-cosine (COS) approximation with coefficients computed directly from the characteristic function 4.3.11. We then sample $X_{t+\Delta}$ by inverting the Cumulative distribution function (CDF) (B.2.2) and set $S_{t+\Delta} = e^{X_{t+\Delta}} - 1$. Integrating the COS density term-wise yields the CDF

$$F^{COS}_{x,\Delta}(\xi) = A_0(\xi - a) + \sum_{k=1}^{N-1} A_k \frac{b-a}{k\pi} sin(k\pi\frac{\xi - a}{b-a}), \qquad \xi \in [a, b], \tag{4.3.14}$$

as shown in B.2.2. Defining the generalised inverse in quantile form we have,

$$Q_{x,\Delta}(u) = \inf\{\xi \in [a, b] : F^{COS}_{x,\Delta}(\xi) \geq u\}, \qquad u \in (0, 1). \tag{4.3.15}$$

By the quantile transform, if $U \sim \text{Unif}(0, 1)$ then,

$$Q_{x,\Delta}(U) \overset{d}{=} X_{t+\Delta} \,|\, X_t = x \quad \text{(Under the COS law)}. \tag{4.3.16}$$

In practice, we evaluate $F^{COS}_{x,\Delta}$ on a grid $a = \xi_0 < \xi_1 < \cdots < \xi_M = b$, set $F_j = F^{COS}_{x,\Delta}(\xi_j)$ (renormalised so that $F_0 = 0, F_M = 1$) and invert piecewise linearly as follows,

$$\text{for } F_j \le u < F_{j+1}: \qquad \widehat{Q}_{x,\Delta}(u) = \xi_j + \frac{u - F_j}{F_{j+1} - F_j}(\xi_{j+1} - \xi_j). \tag{4.3.17}$$

Using this, we are now able to map the price by $S_{t+\Delta} = \exp\{X_{t+\Delta}\} - 1$. Immediately, we notice that as $N \to \infty$ and the window $[a, b]$ expands, the CDF $F^{COS}_{x,\Delta}$ converges to the true transition CDF and since the size $\max_j(\xi_{j+1} - \xi_j) \to 0$ the piecewise linear inverse $\widehat{Q}_{x,\Delta}$ converges to $Q_{x,\Delta}$. Thus this one step draw converges in law to the exact transition $X_{t+\Delta}, \mid X_t = x$. Having now defined a method by which we can simulate the price process, we now attempt to implement this in practice to validate the scheme and present path visualisations and statistics that illustrate the bubble behaviour defined by the strict local martingale attribute of this process.

4.4 Implementation and analysis of a strict local martingale with pure-jumps

We now wish to make the transition law explicit. Using the conditional characteristic function from Lemma 4.3.1 and the COS reconstruction, we approximate the one-step density $f_{x,\Delta}$ and validate this against Monte-Carlo samples. Before we implement this process within python we first specify that all code used within this section can be found in a GitHub repository in Appendix - B under the label jump processes and encourage the reader to experiment with this code. Unless stated otherwise for all runs of code we use $(N, L) = (2048, 20)$, $\Delta = T/n_{\text{steps}}$ and, $t \in [0, T]$ throughout this section.

4.4.1 Validation and numerical refinements

First, since numerically we clamp tiny negative values of f^{COS} to 0 and renormalise its area to 1 to obtain a proper kernel, we wish to verify mass $\int_a^b f^{\text{COS}} \approx 1$ and non-negativity (Figure 4.2), comparing against a histogram of Monte-Carlo draws at the same (x, Δ). To reduce spectral ripples near the left boundary we apply Fejér smoothing ($A_k \leftarrow (1 - k/N)A_k$) and "left padding" (extend a slightly negative in the Fast Fourier Transform grid while keeping the density zero for $\xi < 0$) Gottlieb and Shu (1997); Fang and Oosterlee (2008). These do not materially change moments or the semigroup check but produce visibly smoother densities near a.

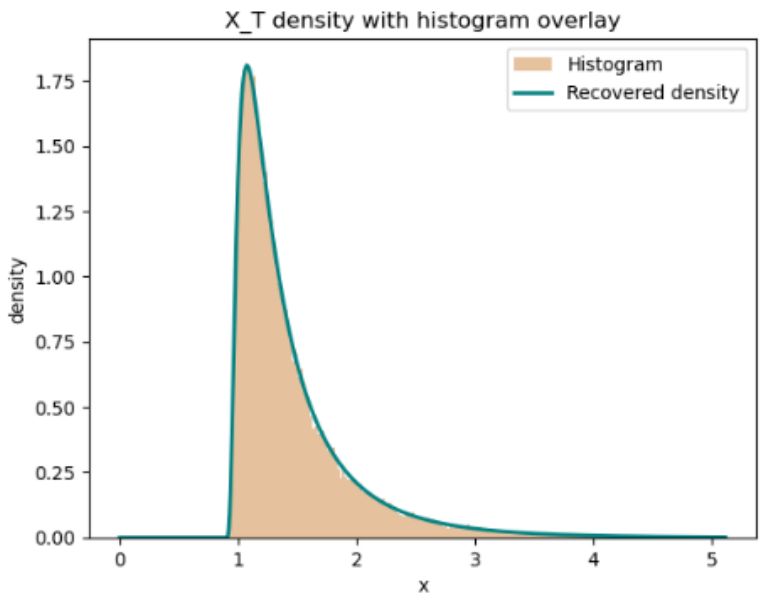

Figure 4.2: Overlay of the COS-recovered transition density f_{X_T} (solid line) and the empirical histogram of X_T obtained by inverse-CDF sampling. The range is truncated at the 99.9% quantile for readability

From Figure 4.2 we can see that the COS-recovered transition density f_{X_T} aligns closely with the histogram of independent, identically distributed samples from X_T. Doing further checks, we find that the density integrates to 1 $\int f_{X_T}\, dx \approx 1$, as expected from classical theory. Taken together, these diagnostics indicate that the recovered density matches the sampling distribution within Monte-Carlo error, as expected when the inverse-CDF is applied to the COS CDF.

Having now validated our code we begin by doing two complementary runs both displayed in Figure 4.3. The parameters for these runs both have $T = 10, \Delta = 1/12$ but differ in intial price S_0 which is 10 and 100 respectively.

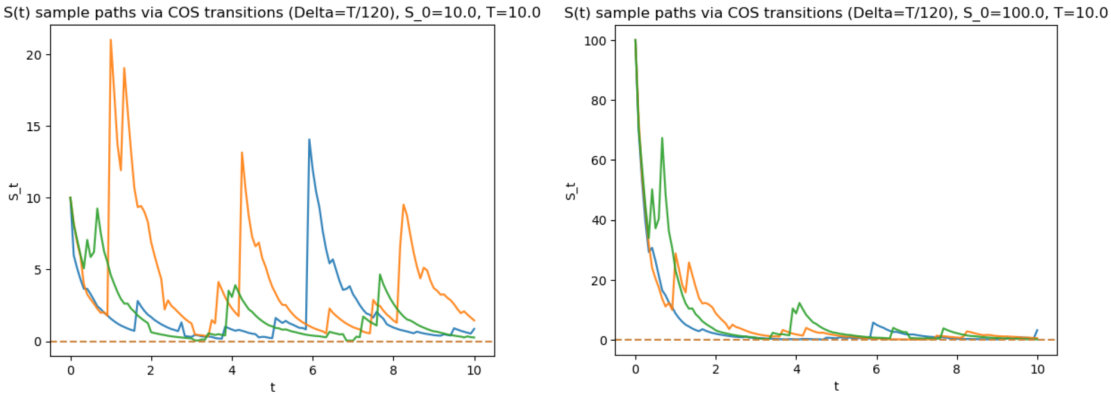

Figure 4.3: Sample paths of the pure-jump price process $S_t = e^{X_t} - 1$ generated with step $\Delta = 1/12$ and $T = 10$. Left: $S_0 = 10$. Right: $S_0 = 100$.

From Figure 4.3 we can see the occasional large, self–exciting jumps of the price $S_t =$

$e^{X_t} - 1$ superimposed on a background of many tiny moves. In our model the small-jump component is of infinite activity, as on any finite interval there are almost surely infinitely many jumps, although their total variation is finite as shown in (4.2.8) - (4.2.9). A time-discretised simulation with step Δ is unable to display all of these jumps, instead, the COS transition $X_{t+\Delta} - X_t$ already aggregates the countably many sub-Δ jumps. In the plot we therefore see only the resolved, ε-large jumps as vertical moves (their exact times lie somewhere inside $(t, t + \Delta]$, while the cloud of sub-ε jumps is represented in aggregate by the thin, jagged "creep." The figure should thus be read as a finite-resolution rendering of a càdlàg path with infinite activity as the big jumps are shown explicitly with the infinitely many tiny ones present but not individually visible. The state-dependent, self-exciting intensity yields clustered upward spikes when the level is high, this is most evident early in the right plot of Figure 4.3 as we observe the activity subsides as the level fall sharply from around 100 to 60. Additionally, consistent with the strict-local-martingale property the paths show a downward pull towards zero as expected from the drift component $B_t(\omega)$ in (4.2.4). Moreover, because $S = e^X - 1$, a jump ΔX_t generates $\Delta S_t = (1 + S_{t^-})(e^{\Delta X_t} - 1) \approx (1 + S_{t^-})\Delta X_t$ the same jump ΔX therefore produces larger price gaps ΔS at higher levels, explaining the outsized early spikes and how they diminish as the path decays. For a fixed maturity T, such rare but sizable jumps imply a right-skewed, heavy tailed law for S_T. Under our strict local martingale setup ($r = d = 0$) this shows the property of $m(t) = S_0 - E[S_t]$ manifestation of the bubble gap used next in this chapter.

4.4.2 Bubble diagnostic: martingale defect $m(t)$

Since we are interested in bubbles we wish to measure the martingale defect (bubble component) $m(t) = S_0 - \mathbb{E}[S_t]$ of the process $S_t = e^{X_t} - 1$ where $x_0 = \ln(1 + S_0)$. Applying 4.3.2 with ($r = d = 0$) we gain the martingale defect for this process as defined,

$$m(t) = S_0 - \mathbb{E}[S_t] = e^{x_0} - \exp(x_0(2e^{-t/2} - e^{-t})) \tag{4.4.1}$$

This process is strict positive for $t > 0$, strictly increasing since $m'(t) = x_0 e^{x_0(2e^{-t/2}-e^{-t})}(e^{-t/2} - e^{-t}) > 0$, and bounded above by S_0. A Taylor expansion at $t = 0$ can be performed to show that $m(t) = \frac{1}{4}e^{x_0}x_0t^2 + \mathcal{O}(t^3)$, so the curve starts flat and grows quadratically before gradually plateauing at S_0 as $T \to \infty$. We see in Figure 4.4 these observations and can see that as $t \to \infty$ the bubble gap $\lim_{t\to\infty} m(t) = S_0$ since $\mathbb{E}[S_t] \to 0$.

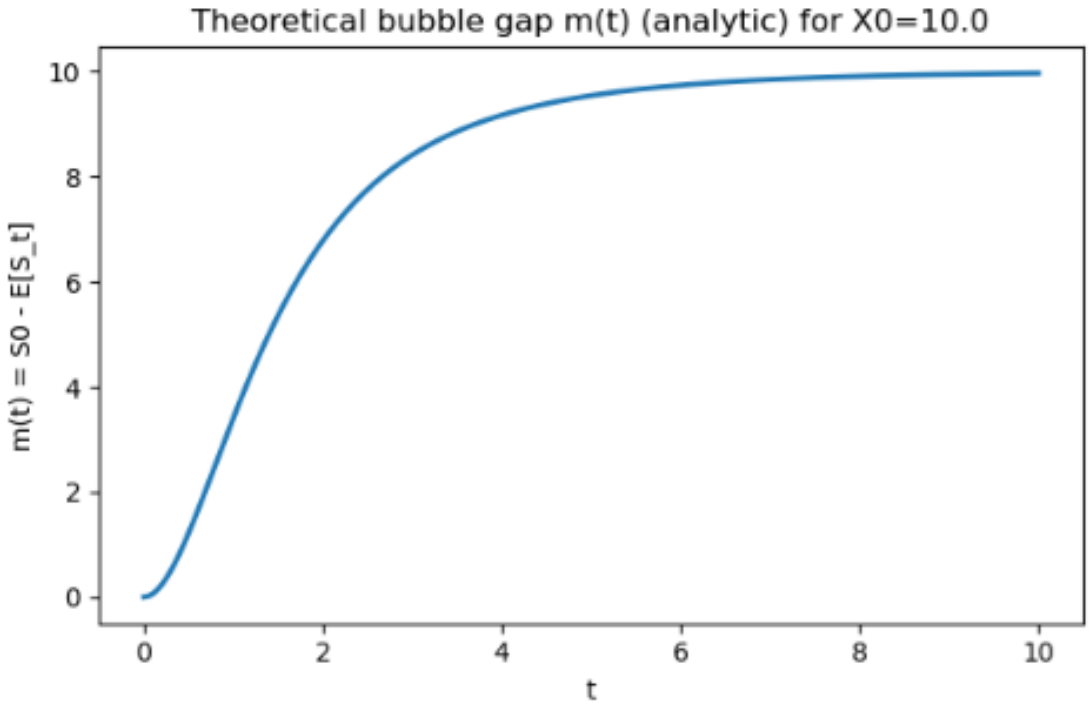

Figure 4.4: Caption

Expanding further from this we now wish to verify that our simulated law repoduces this profile by generating many Monte-Carlo paths via COS transitions and we define the Monte-Carlo estimator as such,

$$\widehat{m}(t) = S_0 = \frac{1}{N}\sum_{i=1}^{N} S_t^{(i)} \tag{4.4.2}$$

with 95% confidence bands. We choose to simulate with initial price $S_0 = 10$, Step size $\Delta = 1/12$, and maturity $T = 10$ with $N = 20$ paths. Figure 4.5 highlights these path processes and their Monte-Carlo mean with the 95% confidence band along with the analytical bubble gap $m(t)$. We can see clearly that the Monte-Carlo mean tracks the theory's path fairly closely when no large jumps are present. When these large jumps do occur there is occasional deviation from the true analytical $m(t)$ due to the increase in variance in the right tail. Theoretically, we could produce many paths of N which would allow the Monte-Carlo estimator to show a closer representation of the analytical bubble gap $m(t)$ but this is limited by the compute power needed for the generation of these paths. Concretely, we can say that for $N \gg 0$ then $\widehat{m}(t) \approx m(t)$.

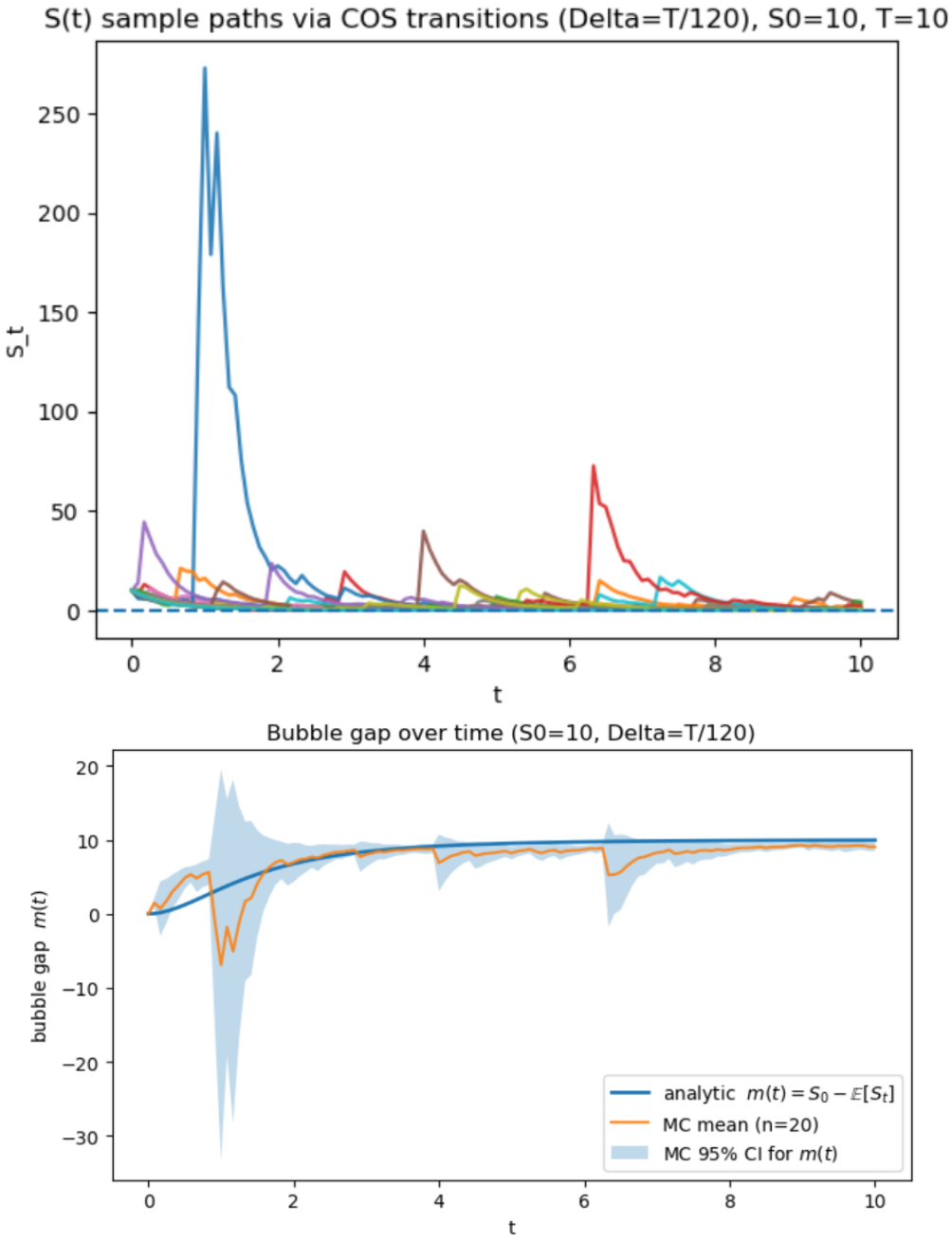

Figure 4.5: Top: Monte-Carlo sample paths of $S_t = e^{X_t} - 1$ generated from COS transition densities ($\Delta = T/120$; $S_0 = 10$, $T = 10$). Bottom: Monte-Carlo estimate of the martingale defect $m(t) = S_0 - \mathbb{E}[S_t]$, analytic $m(t)$, sample mean from $N = 20$ paths, and a pointwise 95% confidence band

4.4.3 Explicit big jumps via an ε–split

Since $S_t = e^{X_t} - 1$ has infinite activity on any finite interval (see (4.2.8)-(4.2.9)), we now design a diagnostic that highlights only the economically significant jump events. Specifically, we apply an ε-split to the one–step transition $Y := X_{t+\Delta} - X_t$: moves with $|Y| > \varepsilon$ are flagged as "large" and displayed explicitly, whereas sub-ε moves are treated as the small-jump background. This labelling is law-preserving, it does not alter the

sampling but it renders the process's self-exciting clustering visible. Our interest lies in these large discontinuities because they drive bubble run-ups and material repricings, while the myriad tiny moves function as high-frequency connective noise between such events. We first let $Y := X_{t+\Delta} - X_t$ denote the one–step increment with CDF $F_{Y|x}(y) = F^{\mathrm{COS}}_{x,\Delta}(x+y)$. We then fix $\varepsilon > 0$ and split the mass into three distinct parts as

$$p_L = \mathbb{P}(Y < -\varepsilon \,|\, X_t = x) = F_{Y|x}(-\varepsilon), \tag{4.4.3}$$

$$p_S = \mathbb{P}(|Y| \leq -\varepsilon \,|\, X_t = x) = F_{Y|x}(\varepsilon) - F_{Y|x}(-\varepsilon), \tag{4.4.4}$$

$$p_R = \mathbb{P}(Y > \varepsilon \,|\, X_t = x) = 1 - F_{Y|x}(\varepsilon), \tag{4.4.5}$$

Here p_L is the left tail mass representing large downward jumps, p_S is the central mass mass representing the myriad of small jumps that appear to make the process look continuous, and p_R is the right tail mass representing the large upward jumps. Now letting $F_{Y|x}$ be the CDF of $Y \,|\, X_t = x$ we can defined renormalised truncated CDFs as such,

$$\begin{aligned}
F_L(y) &= \frac{F_{Y|x}(y)}{p_L}\, \mathbf{1}_{(-\infty,-\varepsilon]}(y), \\
F_S(y) &= \frac{F_{Y|x}(y) - F_{Y|x}(-\varepsilon)}{p_S}\, \mathbf{1}_{(-\varepsilon,\varepsilon]}(y), \\
F_R(y) &= \frac{F_{Y|x}(y) - F_{Y|x}(\varepsilon)}{p_R}\, \mathbf{1}_{[\varepsilon,\infty)}(y).
\end{aligned}$$

From this we can now form the original CDF as the composition of truncated CDFs,

$$F_{Y|x}(y) \;=\; p_L F_L(y) + p_S F_S(y) + p_R F_R(y), \qquad y \in \mathbb{R}.$$

Hence, if $J \in \{L, S, R\}$ is drawn with $\mathbb{P}(J = L) = p_L$, $\mathbb{P}(J = S) = p_S$, $\mathbb{P}(J = R) = p_R$, and then Y^ε is drawn from the conditional law with CDF F_J and we have

$$Y^\varepsilon \;\overset{d}{=}\; Y \mid X_t = x.$$

Equivalently, for any bounded measurable h,

$$\mathbb{E}[h(Y) \mid X_t = x] = p_L\, \mathbb{E}[h(Y) \mid Y < -\varepsilon,\, x] + p_S\, \mathbb{E}[h(Y) \mid |Y| \leq \varepsilon,\, x] + p_R\, \mathbb{E}[h(Y) \mid Y > \varepsilon,\, x].$$

Thus the ε-split does not change our transition law as it only labels which region the increment came from, validating that our split works. Letting $U \sim \mathrm{Unif}(0, 1)$, we can

implement the split via the global CDF $F_{Y|x}$,

$$Y = \begin{cases} F^{-1}_{Y|x}(U), & U \in [0,\, p_L) \quad \text{(left tail)}, \\ F^{-1}_{Y|x}(U), & U \in [p_L,\, p_L + p_S) \quad \text{(small block)}, \\ F^{-1}_{Y|x}(U), & U \in [p_L + p_S,\, 1] \quad \text{(right tail)}. \end{cases}$$

Practically, we compute

$$p_L = F_{Y|x}(-\varepsilon), \qquad p_S = F_{Y|x}(\varepsilon) - F_{Y|x}(-\varepsilon), \qquad p_R = 1 - F_{Y|x}(\varepsilon),$$

from the COS CDF $F^{\text{COS}}_{x,\Delta}$ (shifted by x), and invert linearly on the precomputed grid as in 4.3.17. Plotting one realisation and setting $\varepsilon = 0.25, S_0 = 10$, $T = 1$ with 125 steps, (therefore $\Delta = \frac{1}{125}$), we obtain the plots as in 4.6.

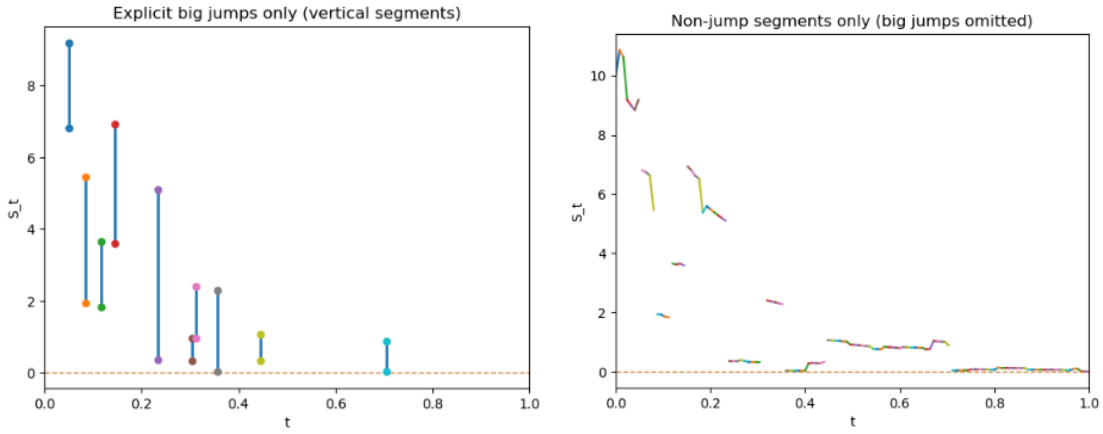

Figure 4.6: Two plots that show the same path of $S_t = e^{X_t} - 1$ with $t = 1, S_0 = 10, \Delta = 1/125, \varepsilon = 0.25$. Left: Vertical segments mark the large jumps (plotted at a uniform time inside each step) with dots showing pre and post jump levels. Right: Only the small jump that connect between the large jumps are drawn.

From 4.6 we can explicitly see the times at which the big jumps in the price process $S_t = e^{X_t} - 1$ occur. Mathematically, the large jumps represent sudden price gaps that occur instantaneously, causing a break in the data and are closely related to real markets as they mirror discrete information arrivals, where sudden information shocks such as earnings surprises and policy announcements produce sudden price gaps in practice. The self-exciting intensity is observable as well and captures the observed feedback of momentum and herding. As the prices rise, jump intensity rises along with it, increasing the change of further abrupt moves. This is why we tend to observe much bigger gaps at higher values. Figure 4.6 also validates the theory by making the models structure of 4.2.8-4.2.9 observable, as we can clearly see the small "infinite" jumps that carry the process between the sharp meaningful jumps. The reason we are interested in observing these is due to the fact that market prices tend not be on a continuous scale and as such

will hold discontinuities. For example, where a stock is priced in units of 0.01 as the lowest denomination, we immediately see that there will be a discontinuity in data between two values such as 0.01 and 0.02. This is why being able to model discontinuous bubble behaviour is of empirical importance to us, as it aligns with the discontinuities apparent in real markets. Being able to theoretically show this, one could perhaps extend this study further to develop a more robust model and implement this onto real market data.

Chapter 5

Conclusion

This dissertation has developed a comprehensive, option implied codebase available for real time detection and quantification of asset price bubbles. By synthesizing martingale theory, nonparametric option-price bounds, and self exciting jump process dynamics, it delivers both theoretical insight and practical algorithms suitable for live markets. Making our code pipeline and findings of interest to both researchers within this space and market practitioners who wish to infer if a bubble is potentially be present.

First, rigorous martingale defect estimators were derived from put call parity and tail integral representation, yielding three complementary empirical tests. These include, mean shortfall estimation via Monte Carlo, far OTM tail averaging on a decreasing convex call fit, and strike window integration under Delta bands. Across Black-Scholes, CEV and SABR models, these estimators correctly distinguished between true martingales and strict local martingales, recovering known bubble gaps without modelling assumptions beyond no arbitrage. Applying the Delta band estimator to market Nvidia option sheets revealed a statistically significant martingale defect across short to normal times until maturity as compared to longer maturities, with ATM and ITM bands being the most robust in all cases. This provides actionable signals for risk managers and regulators to flag potential bubble pressures before they occur. Extending beyond continuous models, a novel pure jump self exciting affine process was introduced and implemented via COS-based simulation. This process generates clustered upward jumps and a persistent martingale gap, mirroring real world discontinuities and feedback loops, characteristic of speculative manias. Together, these contributions establish a fully implementable framework for bubble detection using only observable quotes. In practice, risk desks can calibrate call curve fits each trading day estimate the bubble gap across maturities and Delta bands, and monitor its evolution as an early-warning indicator. From this thesis, we could expand in a number of directions, one being through an intra-day bubble indicator. Collecting high frequency quotes and fitting an arbitrage free call surface to extract the strike independent tail, from this we could track this tail through the day to detect sudden spikes around macro announcements or earnings. Secondly, we could extend the self-exciting pure-jump model

to two assets with mutually amplifying jump intensities. deriving conditions under which joint strict local martingale behaviour emerges. Thirdly, building on the no arbitrage partial identification approach to derive $m(T)$ bounds when bid ask spreads and discrete hedging costs are present. we could potentially prove that under a bounded proportional transaction cost, the strike independent plateau persists within ε-tolerance. This thesis not only advances academic understanding of strict local martingales but also equips practitioners with forward looking metrics to manage speculative excess and safeguard financial stability.

Appendices

Appendix A

Simulation details and proofs

Proposition A.0.1 (GBM closed form and expectation)**.** *Let S solve $\mathrm{d}S_t = \sigma S_t \,\mathrm{d}W_t$ with $S_0 > 0$ and $\sigma > 0$. Then*

$$S_T = S_0 \exp\Big(\sigma W_T - \frac{1}{2}\sigma^2 T\Big) \quad \textit{and} \quad \mathbb{E}[S_T] = S_0.$$

Proof. Fix $T > 0$ and define the localising times $\tau_n := \inf\{t \le T : \, S_t \le 1/n\} \wedge T$. Apply Itô to $f(s) = \log s$ on $[0, t \wedge \tau_n]$:

$$\log S_{t\wedge\tau_n} - \log S_0 = \int_0^{t\wedge\tau_n} \frac{1}{S_u}\,\mathrm{d}S_u - \frac{1}{2}\int_0^{t\wedge\tau_n} \frac{1}{S_u^2}\,\mathrm{d}\langle S\rangle_u = \sigma W_{t\wedge\tau_n} - \frac{1}{2}\sigma^2(t\wedge\tau_n),$$

since $\mathrm{d}\langle S\rangle_u = \sigma^2 S_u^2\,\mathrm{d}u$. Letting $n \to \infty$ (standard localisation) yields $\log S_t = \log S_0 + \sigma W_t - \frac{1}{2}\sigma^2 t$ for all $t \le T$, hence the stated closed form and $S_t > 0$ a.s. Because $W_T \sim \mathcal{N}(0, T)$, $\mathbb{E}[\exp(\sigma W_T - \frac{1}{2}\sigma^2 T)] = 1$, so $\mathbb{E}[S_T] = S_0$. □

Appendix B

Abate-Whitt and COS reconstruction

B.1 Bromwich inversion via the trapezoidal rule (following Abate–Whitt)

Let $F(s) = \int_0^\infty e^{-sx} f(x)\,dx$ be the Laplace transform of a density f. The Bromwich inversion reads

$$f(x) = \frac{1}{2\pi i} \int_{\sigma - i\infty}^{\sigma + i\infty} e^{sx} F(s)\,ds, \qquad \gamma > 0. \tag{B.1.0}$$

Following Abate and Whitt (1992), we evaluate this integral numerically by applying the trapezoidal quadrature rule,

$$\int_a^b g(v)\,dv \;\approx\; h\left[\frac{1}{2}\,g(a) \;+\; \sum_{k=1}^{M-1} g(a+kh) \;+\; \frac{1}{2}\,g(b)\right], \qquad h = \frac{b-a}{M}, \tag{B.1.1}$$

to the vertical contour after the change of variables $s = (A + iv)/x$, which yields

$$f(x) = \frac{e^{A/x}}{2\pi x} \int_{-\infty}^{\infty} e^{iv}\, F\!\left(\frac{A+iv}{x}\right) dv. \tag{B.1.2}$$

Sampling at $v_k = 2\pi k$ and truncating at $|k| \leq K$ gives the standard alternating "Fourier-series" approximation ,

$$f(x) \;\approx\; \frac{e^{A/2}}{x}\left[\frac{1}{2}\Re\, F\!\left(\frac{A}{x}\right) \;+\; \sum_{k=1}^{K} (-1)^k\, \Re\, F\!\left(\frac{A + k\pi i}{x}\right)\right]. \tag{B.1.3}$$

Where A is the vertical line shift of the Bromwich contour and K is the number of trapezoidal samples in the Fourier-series sum.

B.2 Fourier–cosine (COS) reconstruction for transitions

Let Z be a real random variable with characteristic function $\phi_Z(\omega) = \mathbb{E}[e^{i\omega Z}]$. Fix a truncation interval $[a, b]$ that contains (almost) all probability mass of Z then from Fang and Oosterlee (2008), the coefficients and density on $[a, b]$ are,

$$A_k = \frac{2}{b-a} \Re\left\{ \phi_Z\Big(\frac{k\pi}{b-a}\Big)\, e^{-ik\pi a/(b-a)} \right\}, \qquad k = 0, 1, \ldots, N-1, \tag{B.2.0}$$

(with A_0 taken at half weight), and

$$f^{\mathrm{COS}}(x) = \sum_{k=0}^{N-1} A_k \cos\Big(k\pi \frac{x-a}{b-a}\Big), \qquad x \in [a, b]. \tag{B.2.1}$$

The CDF (termwise integral) is as defined,

$$F^{\mathrm{COS}}(x) = A_0(x-a) + \sum_{k=1}^{N-1} A_k \frac{b-a}{k\pi} \sin\Big(k\pi \frac{x-a}{b-a}\Big). \tag{B.2.2}$$

If $\kappa(u) = \log \mathbb{E}[e^{uZ}]$ exists near $u = 0$ with $c_1 = \kappa'(0)$ and $c_2 = \kappa''(0)$, then the generic cumulant window (two–sided support) is

$$a = c_1 - L\sqrt{c_2}, \qquad b = c_1 + L\sqrt{c_2}, \qquad L \in [8, 20]. \tag{B.2.3}$$

When ϕ_Z is analytic on a strip around the real axis, the COS error decays exponentially in N, while truncation bias is controlled by $[a, b]$ (cf. Fang and Oosterlee (2008)).

Appendix C

Local Taylor expansion ($t = 0$)

C.1 Local Taylor expansion ($t = 0$)

Using Taylor's theorem with remainder (see Apostol, 1974, Ch. 7) and the Maclaurin series for the exponential (Olver et al., 2010–, Section 4.2), we expand $e^{-t/2}$ and e^{-t} about $t = 0$. Retaining terms up to t^3 yields $m(t) = \frac{1}{4} e^{x_0} x_0 \, t^2 + \mathcal{O}(t^3)$.

Recall that $S_t = e^{X_t} - 1$, $x_0 = \ln(1 + S_0)$, and

$$m(t) \;:=\; S_0 - \mathbb{E}[S_t] \;=\; e^{x_0} - \exp(x_0(2e^{-t/2} - e^{-t})).$$

we claim that as $t \downarrow 0$,

$$m(t) \;=\; \frac{1}{4} e^{x_0} x_0 \, t^2 \;-\; \frac{1}{8} e^{x_0} x_0 \, t^3 \;+\; \mathcal{O}(t^4), \tag{C.0.1}$$

in particular $m(0) = 0$, $m'(0) = 0$, and $m''(0) = \frac{1}{2} e^{x_0} x_0 > 0$.
Using the Maclaurin series,

$$e^{-t/2} = 1 - \frac{t}{2} + \frac{t^2}{8} - \frac{t^3}{48} + \mathcal{O}(t^4), \qquad e^{-t} = 1 - t + \frac{t^2}{2} - \frac{t^3}{6} + \mathcal{O}(t^4),$$

we obtain,

$$2e^{-t/2} - e^{-t} = 1 - \frac{t^2}{4} + \frac{t^3}{8} + \mathcal{O}(t^4).$$

Hence

$$\exp(x_0(2e^{-t/2} - e^{-t})) = e^{x_0} \exp\Big(x_0\Big[-\frac{t^2}{4} + \frac{t^3}{8} + \mathcal{O}(t^4)\Big]\Big) = e^{x_0}\Big(1 - \frac{x_0}{4}t^2 + \frac{x_0}{8}t^3 + \mathcal{O}(t^4)\Big),$$

since the square of the bracket contributes $O(t^4)$. Therefore as in C.0.1,

$$m(t) = e^{x_0} - e^{x_0}\Big(1 - \frac{x_0}{4}t^2 + \frac{x_0}{8}t^3 + \mathcal{O}(t^4)\Big) = \frac{1}{4} e^{x_0} x_0 \, t^2 - \frac{1}{8} e^{x_0} x_0 \, t^3 + \mathcal{O}(t^4).$$

Appendix D

Codebase and data

Any figure generated within this document along with respective sheets of information that these may use, can be found in the GitHub repository labeled Financial-Bubbles-Dissertaion-Code - `https://github.com/ej736/Financial-Bubbles-Dissertaion-Code`

Bibliography

Abate, J. and Whitt, W., 1992. The fourier-series method for inverting transforms of probability distributions. *Queueing systems* [Online], 10(1-2), pp.5–88. Available from: https://doi.org/10.1007/BF01158520.

Apostol, T.M., 1974. *Mathematical analysis*. 2nd ed. Taylor's theorem with remainder. Addison–Wesley.

Applebaum, D., 2009. *Lévy processes and stochastic calculus* [Online], *Cambridge studies in advanced mathematics*, vol. 116. 2nd ed. See Example 1.3.8 and Chapter 3. Cambridge: Cambridge University Press. Available from: https://doi.org/10.1017/CBO9780511809781.

Biagini, F., Gonon, L., Mazzon, A. and Meyer-Brandis, T., 2024. Detecting asset price bubbles using deep learning. *Mathematical finance* [Online], 35(1), pp.74–110. Available from: https://doi.org/10.1111/mafi.12443.

Black, F. and Scholes, M., 1973. The pricing of options and corporate liabilities. *Journal of political economy* [Online], 81(3), pp.637–654. Available from: https://doi.org/10.1086/260062.

Cboe, 2025. *Nvda options — delayed quotes (quote table)* [Online]. Cboe. Available from: https://www.cboe.com/delayed_quotes/nvda/quote_table [Accessed 2025-09-10].

Cox, A. and Hobson, D., 2005. Local martingales, bubbles and option prices. *Finance and stochastics* [Online], 9(4), pp.477–492. Available from: https://ideas.repec.org/a/spr/finsto/v9y2005i4p477-492.html [Accessed 20/05/2025].

Delbaen, F. and Schachermayer, W., 1994. A general version of the fundamental theorem of asset pricing. *Mathematische annalen*, 300(1), pp.463–520.

Delbaen, F. and Shirakawa, H., 2002. No arbitrage condition for positive diffusion price processes. *Asia-pacific financial markets* [Online], 9(3), pp.159–168. Available from: https://doi.org/10.1023/A:1016005714625.

Duffie, D., Filipović, D. and Schachermayer, W., 2003. Affine processes and applications in finance. *The annals of applied probability* [Online], 13(3), pp.984–1053. Available from: https://doi.org/10.1214/aoap/1060202833.

Dupire, B., 1994. Pricing with a smile. *Risk*, 7(1), pp.18–20.

Fang, F. and Oosterlee, C.W., 2008. A novel pricing method for european options based on fourier–cosine series expansions. *Siam journal on scientific computing* [Online], 31(2), pp.826–848. Available from: https://doi.org/10.1137/080718061.

Gilles, C., 1989. Charges as equilibrium prices and asset bubbles. *Journal of mathematical economics*, 18(2), April, pp.155–167.

Gottlieb, D. and Shu, C.W., 1997. On the gibbs phenomenon and its resolution. *Siam review*, 39(4), pp.644–668.

Hagan, P., Lesniewski, A. and Woodward, D., 2015. Probability distribution in the SABR model of stochastic volatility. In: P.K. Friz, J. Gatheral, A. Gulisashvili, A. Jacquier and J. Teichmann, eds. *Large deviations and asymptotic methods in finance* [Online]. Cham: Springer, *Springer proceedings in mathematics & statistics*, vol. 110, pp.1–35. Available from: https://doi.org/10.1007/978-3-319-11605-1_1.

Hull, J. and White, A., 1987. The pricing of options on assets with stochastic volatilities. *The journal of finance* [Online], 42(2), pp.281–300. Available from: https://doi.org/10.1111/j.1540-6261.1987.tb02568.x.

Itkin, A., 2020. Local volatility and dupire's equation. *Fitting local volatility: Analytic and numerical approaches in black–scholes and local variance gamma models* [Online]. World Scientific, pp.3–12. Available from: https://doi.org/10.1142/9789811212772_0001.

Jacod, J. and Shiryaev, A.N., 1987. *Limit theorems for stochastic processes*, *Grundlehren der mathematischen wissenschaften*, vol. 288. 1st ed. Berlin Heidelberg: Springer.

Jarrow, R.A., Kchia, Y. and Protter, P., 2011. How to detect an asset bubble. *Siam journal on financial mathematics* [Online], 2(1), pp.839–865. Available from: https://doi.org/10.1137/10079673X.

Jarrow, R.A. and Kwok, S.S., 2021. Inferring financial bubbles from option data. *Journal of applied econometrics* [Online], 36(7), pp.1013–1046. Available from: https://doi.org/10.1002/jae.2862.

Jarrow, R.A., Protter, P. and Shimbo, K., 2006. Asset price bubbles in complete markets. *Advances in mathematical finance* [Online]. Birkhäuser Boston, Applied and Numerical Harmonic Analysis, pp.97–121. Available from: https://doi.org/10.1007/978-0-8176-4545-8_7.

Jarrow, R.A., Protter, P. and Shimbo, K., 2010. Asset price bubbles in incomplete markets. *Mathematical finance* [Online], 20(2), pp.145–185. Available from: https://doi.org/10.1111/j.1467-9965.2010.00394.x.

Keller-Ressel, M., 2015. Simple examples of pure-jump strict local martingales. *Stochastic processes and their applications* [Online], 125(11), pp.4142–4153. Available from: https://doi.org/10.1016/j.spa.2015.06.003.

Kindleberger, C.P. and Aliber, R.Z., 2005. *Manias, panics, and crashes: A history of financial crises*, Wiley Investment Classics. 5th ed. Foreword by Robert M. Solow. Hoboken, NJ: John Wiley & Sons.

Malkiel, B.G., 2019. *A random walk down wall street*. 12th ed. New York: W. W. Norton & Company.

Merton, R.C., 1976. Option pricing when underlying stock returns are discontinuous. *Journal of financial economics* [Online], 3(1–2), pp.125–144. Available from: https://doi.org/10.1016/0304-405X(76)90022-2.

Mijatović, A. and Urusov, M., 2012. On the martingale property of certain local martingales. *Probability theory and related fields* [Online], 152(1-2), pp.1–30. Available from: https://doi.org/10.1007/s00440-010-0314-7.

Ofek, E. and Richardson, M., 2003. Dotcom mania: The rise and fall of internet stock prices. *The journal of finance* [Online], 58(3), June, pp.1113–1137. Available from: https://doi.org/10.1111/1540-6261.00560.

Øksendal, B., 2003. *Stochastic differential equations: An introduction with applications*. 6th ed. Springer.

Olver, F.W.J., Lozier, D.W., Boisvert, R.F. and Clark, C.W.e., 2010–. *Nist digital library of mathematical functions* [Online]. Exponential function Maclaurin series, §4.2. Available from: https://dlmf.nist.gov/4.2.

Protter, P., 2015. Strict local martingales with jumps. *Stochastic processes and their applications* [Online], 125(4), pp.1352–1367. Available from: https://doi.org/10.1016/j.spa.2014.10.018.

Revuz, D. and Yor, M., 1999. *Continuous martingales and brownian motion* [Online], *Grundlehren der mathematischen wissenschaften*, vol. 293. 3rd ed. Berlin: Springer. Available from: https://doi.org/10.1007/978-3-662-06400-9.

Rogers, L.C.G. and Williams, D., 2000. *Diffusions, markov processes and martingales: Volume 1, foundations*, Cambridge Mathematical Library. 2nd ed. See Chapter II.2. Cambridge: Cambridge University Press.

Sabanis, S., 2016. Euler approximations with varying coefficients: the case of diffusion coefficients with superlinear growth. *The annals of applied probability*, 26(4), pp.2083–2105.

Shiller, R.J., 2000. *Irrational exuberance*. 1st ed. Princeton, NJ: Princeton University Press.

Singh, M., 2024. The 2008 financial crisis explained [[Online]] [Online]. Available from: https://www.investopedia.com/articles/economics/09/financial-crisis-review.asp [Accessed 11/05/2025].

Sornette, D. and Cauwels, P., 2014. Financial bubbles: Mechanisms and diagnostics [Online]. Notenstein White Paper Series; Swiss Finance Institute Research Paper No. 14-28. 1404.2140, Available from: https://doi.org/10.48550/arXiv.1404.2140.

Trading Economics, 2025. *United states interest rate* [Online]. Trading Economics. Available from: https://tradingeconomics.com/united-states/interest-rate [Accessed 2025-09-10].

Yan, Y., 2023. *Financial bubble prediction with neural networks* [Online]. MSc Mathematical Finance thesis. Master's thesis. Imperial College London, Department of Mathematics. Available from: https://www.imperial.ac.uk/media/imperial-college/faculty-of-natural-sciences/department-of-mathematics/math-finance/212266979---Yan-Yuchen-Yan---Yan_Yuchen_02292404.pdf.